ORNL
MASTER COPY

OAK RIDGE NATIONAL LABORATORY

operated by

UNION CARBIDE CORPORATION

for the

U.S. ATOMIC ENERGY COMMISSION

ORNL-TM-33

CHEMICAL TECHNOLOGY DIVISION

UNIT OPERATIONS SECTION

MONTHLY PROGRESS REPORT

MAY 1961

NOTICE

This document contains information of a preliminary nature and was prepared primarily for internal use at the Oak Ridge National Laboratory. It is subject to revision or correction and therefore does not represent a final report. The information is not to be abstracted, reprinted or otherwise given public dissemination without the approval of the ORNL patent branch, Legal and Information Control Department.

LEGAL NOTICE

This report was prepared as an account of Government sponsored work. Neither the United States, nor the Commission, nor any person acting on behalf of the Commission:

A. Makes any warranty or representation, expressed or implied, with respect to the accuracy, completeness, or usefulness of the information contained in this report, or that the use of any information, apparatus, method, or process disclosed in this report may not infringe privately owned rights; or

B. Assumes any liabilities with respect to the use of, or for damages resulting from the use of any information, apparatus, method, or process disclosed in this report.

As used in the above, "person acting on behalf of the Commission" includes any employee or contractor of the Commission, or employee of such contractor, to the extent that such employee or contractor of the Commission, or employee of such contractor prepares, disseminates, or provides access to, any information pursuant to his employment or contract with the Commission, or his employment with such contractor.

ORNL-TM-33

UNIT OPERATIONS SECTION MONTHLY PROGRESS REPORT

May 1961

CHEMICAL TECHNOLOGY DIVISION

M. E. Whatley

P. A. Haas
R. W. Horton
A. D. Ryon
J. C. Suddath
C. D. Watson

Date Issued

DEC 26 1961

OAK RIDGE NATIONAL LABORATORY
Oak Ridge, Tennessee
Operated By
UNION CARBIDE CORPORATION
for the
U. S. Atomic Energy Commission

ABSTRACT

The experimental results on the oxidation of hydrogen from a helium stream with copper oxide pellets were very close to the predicted behavior based on the mathematical model. Experimental measurements of uranyl sulfate loading rates on chloride equilibrated resin showed little variation with solution concentrations. A tentative flowsheet was proposed for cost analysis of processing a Pebble Bed Reactor. A uranium-zirconium plate was dissolved in nitrate-free Zirflex solution. An authentic TRIGA prototype was processed in engineering-scale equipment. Three 4-stage leacher model dissolution runs were made, two of which used 8 M HNO_3 and one used 4 M HNO_3. Flooding rates and holdup data were obtained for sieve plate pulse columns under 5% TBP-1.8 M $Al(NO_3)_3$ flowsheet conditions. A Purex waste calcination run (R-37) was made using sodium and magnesium to reduce sulfate volatility.

CONTENTS

		Page
	Abstract	2
	Previous Reports in this Series for the Years 1960-1961	4
	Summary	5
1.0	GCR Coolant Purification Studies	7
2.0	Ion Exchange	17
3.0	Power Reactor Fuel Processing	20
4.0	Solvent Extraction Studies	30
5.0	Waste Processing	41

Previous Reports in this Series for the Years 1960-1961

January	ORNL CF 60-1-49
February	ORNL CF 60-2-56
March	ORNL CF 60-3-61
April	ORNL CF 60-4-37
May	ORNL CF 60-5-58
June	ORNL CF 60-6-11
July	ORNL CF 60-7-46
August	ORNL CF 60-8-86
September	ORNL CF 60-9-43
October	ORNL CF 60-10-49
November	ORNL CF 60-11-38
December	ORNL CF 60-12-28
January	ORNL CF 61-1-27
February	ORNL CF 61-2-65
March	ORNL CF 61-3-67
April	ORNL-TM-32

All previous reports in this series are listed in CF 60-6-11, from the beginning, December 1954.

SUMMARY

1.0 GCR COOLANT PURIFICATION STUDIES

Predicted results of hydrogen oxidation by copper oxide pellets based on a model of external and internal diffusion were in good agreement with experimental results. Experimental results are calculated based on flow rates and concentrations measured to $\pm$ 5%, and the agreement with predicted results was within experimental error.

2.0 ION EXCHANGE

Experimental measurements of uranyl sulfate loading rates on chloride equilibrated 960 micron Dowex 21K showed little variation with the loading solution uranium and sulfate concentrations. According to a proposed kinetic model, this would indicate little variation in the equilibrium uranium to sulfate loading ratio over this concentration range.

Predicted chloride elution rates from 820 micron resin during uranyl sulfate loading were in good agreement with experimental measurements when at equilibrium 0.98 of the effective resin capacity was assumed to be occupied with $UO_2(SO_4)_2^{=}$ at the remainder with sulfate ions.

3.0 POWER REACTOR FUEL PROCESSING

3.1 U-C Fuel Processing

As the basis for cost analysis of processing a Pebble Bed Reactor fuel containing ~10% ThC_2, UC_2 dispersed in graphite spheres, a tentative flowsheet was calculated which involves the loss to waste streams of 1.15 liter of 22.5 M HNO_3 (equivalent) per kg of graphite fuel. The reference dissolver is an upright slab with moderate gas overpressure to drive a continuous flow of acid downward through the bed disintegrated fuel.

3.2 Modified Zirflex

In engineering-scale equipment 1/8-in. thick 8% U-Zr plate was dissolved in 2 hrs in refluxing dissolvent initially 6.53 M NH_4F-0.1 M H_2O_2 (run CZr-5); there was no stable foam although H_2 was evolved in the ratio of 2 moles H_2/mole Zr dissolved. The scrubbed "off-gas" contained $H_2 + H_2O \cong 99\%$ with $O_2 \leqq 0.15\%$.

An authentic TRIGA prototype (normal U) was processed in the engineering-scale equipment. The 0.030-in. Al cladding and the Al-Sn poison discs were dissolved in < 30 min in refluxing 2 M NaOH-1.8 M $NaNO_3$. About two thirds (by wt) of the two graphite slugs were disintegrated in 2 hrs in 90 vol % HNO_3 (white fuming)- 10 vol % H_2SO_4 (fuming) at room temperature. The 8% U-ZrH meat slug (1.4-in. dia x 14-in. long) weighing 2274 g was 99.75% dissolved after 11-1/2 hrs refluxing in dissolvent initially 6.3 M NH_4F-0.55 M NH_4NO_3-0.01 M H_2O_2.

Acid-aluminum stabilized solvent extraction feed solution containing 0.46 M Zr, 0.78 M free F^-, 3.44 g U/liter and 0.8 M HNO_3 and $Al(NO_3)_3$, and H_2O stabilized solutions containing 0.444 M Zr, 0.62 M free F^-, and 3.54 g U/liter remained stable after > 300 hrs at room temperature.

3.3 Shearing and Leaching

A four stage leacher model dissolution run in which 9 batches of UO_2 pellets (600 g/batch) were dissolved using 4 M HNO_3 at a HNO_3/UO_2 mole ratio of 5.43 as the dissolvent resulted in 98.4 - 99.3% of the UO_2 dissolved in a 4 hr dissolution time.

Two four-stage leacher model dissolution runs in which 9 batches of UO_2 pellets (600 g/batch) were dissolved in each using 8 M HNO_3 as the dissolvent resulted in a steady-state composite product of 500 g U/liter and 1.9 M H^+ at a HNO_3/UO_2 mole ratio of 4 as compared to a composite product of 335 g U/liter and 4.1 M H^+ at a HNO_3/UO_2 mole ratio of 6.15. In each run apparent steady state was attained in 3 - 4 batches.

4.0 SOLVENT EXTRACTION STUDIES

Flooding rates and holdup data were obtained for sieve plate (0.125-in.-dia holes, 23% free area) pulse columns under 5% TBP-1.8 M $Al(NO_3)_3$ flowsheet conditions. Maximum capacity of the compound extraction scrub column was 2010 gal $ft^{-2}hr^{-1}$ for aqueous continuous operation at 50 cpm. Increasing the ratio of dispersed phase to continuous phase from 3/10 to 3/1 while holding the pulse frequency constant at 70 cpm lowered the flooding rate from 933 to 287 gal $ft^{-2}hr^{-1}$. Flooding data was correlated by a method based on hindered settling whereby phase flow rates were related to dispersed phase holdup by the characteristic droplet velocity. Actual and theoretical phase flow velocities at flooding agreed well at 3/10 phase ratio. However, as the ratio of dispersed phase to the continuous phase increased, the theoretical velocities became progressively greater than those actually measured. Measurements showed that dispersed phase holdup varied markedly throughout the column, probably due to surface effect of the plates, resulting in increased holdup at the higher dispersed to continuous phase ratio.

5.0 WASTE PROCESSING

The feed used for test R-37 was Purex 1WW plus 1.2 M Na and 0.2 M Mg added to reduce sulfate volatility. There was serious corrosion of the calciner pot in the area of the liquid level. The solid was partially melted and separated. The corrosion was probably increased because of loss of temperature control because a thermocouple corroded and allowed the calciner pot outside temperature to reach a temperature greater than 1100°C. The overheating may have decomposed some $MgSO_4$ (decomposed in 900°C) allowing SO_3 to attack the 304 stainless steel calciner pot.

The test controlled, except for one temperature zone, very well. The evaporator controlled as had been predicted.

1.0 GCR COOLANT PURIFICATION STUDIES

J. C. Suddath

Contamination of coolant gases by chemical impurities and release of fission products from fuel elements are major problems in gas-cooled reactors and in-pile experimental loops. Investigations are being made to determine the best methods to reduce the impurities, both radioactive and non-radioactive, with emphasis on the kinetics of the fixed bed oxidation of hydrogen by copper oxide.

An attempt is being made to fit experimental data from the study of the $CuO-H_2$ reaction to a mathematical model of external diffusion and internal diffusion of H_2 controlling the rapid, irreversible reaction of H_2 with CuO.

1.1 Comparison Between Predicted Results and Experimental Data - C. D. Scott

The method used to test the mathematical model with experimental data was to compare results predicted by the mathematical model with actual experimental data.

The deep-bed tests in which 1/2-in. to 2-in. deep beds of CuO pellets were used to oxidize H_2 in a flowing stream of helium were run for this purpose (Unit Operations Monthly Reports for January, February, and March, 1961). In these tests, the effluent hydrogen concentration was measured periodically to give complete effluent hydrogen concentration histories. The differential equations derived for the external diffusion-internal diffusion rate controlling model were used to calculate the effluent hydrogen concentration history.

1.2 Solution of Differential Equations

The three differential equations which describe the external diffusion-internal diffusion model are: (March 1961 Unit Operations Monthly Report)

Deep bed material balance,

$$\left(\frac{\partial C}{\partial t}\right)_z + V\left(\frac{\partial C}{\partial z}\right)_t = -\frac{1}{\beta}\left(\frac{\partial n}{\partial t}\right)_z \qquad (1)$$

Reaction rate,

$$\left(\frac{\partial n}{\partial t}\right)_z = k_g\, a\, C \left[1 - \frac{k_g\, a}{\tau}\left(\frac{R - r_o}{4\pi\alpha\, r_o R + \frac{k_g\, a}{\tau}\left(R - r_o\right)}\right)\right] \qquad (2)$$

Position of Cu-CuO interface,

$$\frac{r_o}{R}\left[4\pi\alpha D R r_o + \frac{k_g\, a}{\tau}\left(R - r_o\right)\right] dr_o = -\frac{\alpha D k_g\, a\, C}{b\tau}\, dt \qquad (3)$$

where,

C = bulk gas-phase hydrogen concentration, g-moles/cc

t = time of reaction, sec

z = height in fixed bed of CuO measured from the bottom of the bed, cm

V = linear velocity through the interstices between CuO pellets, cm/sec

β = bed porosity, volume of intergranular voids per unit gross volume of bed

n = g-moles of CuO which have been reacted to Cu in a unit volume of bed, g-moles/cc

k_g = mass-transfer coefficient across the external gas film, cm/sec

a = superficial surface of the CuO pellet per unit volume of bed, cm^2/cm^3

τ = number of CuO pellets in a unit volume of bed, pellets/cc

R = radius of a sphere having the same volume as the average volume of the CuO pellets, cm

r_o = radius of the Cu-CuO interface in a pellet, cm

α = effective internal porosity of the Cu pellet, void volume/total volume

D = molecular diffusivity of hydrogen in helium at the conditions of the system, cm^2/sec

b = molar density of CuO in the CuO pellets, g-moles/cc

These equations can be solved simultaneously by a finite difference method and the hydrogen concentration in the effluent gas stream can be predicted as a function of time. For a finite difference solution, the position of the Cu-CuO interface, r_o, can be determined by a relation, somewhat simpler than equation (3). The change in r_o during a short period of time can be determined by:

$$dr_o = \frac{dt}{4\alpha r_o^2 \tau}\left(\frac{\partial n}{\partial t}\right)_z \qquad (4)$$

The finite-difference solution of equations (1), (2) and (4) was set up for a high-speed digital computer and seven different cases were solved.

By use of these equations one finds qualitatively that a plot of C/C_o (effluent H_2 concentration/initial H_2 concentration) vs time gives the typical "S"-shaped curve found in the experimental tests. When the measured value of the effective porosity (April 1961 Unit Operations Monthly Report) was used along with the initial experimental conditions, the predicted effluent hydrogen concentration for six deep bed runs gave fair agreement with experimental values and in three particular cases (runs R-4, R-7 and R-9) the agreement was very good (Figures 1.1, 1.2, 1.3, 1.4, 1.5, 1.6, and 1.7). Since these predicted values are based on gas flow rates, and initial hydrogen concentrations measured to $\pm$ 5%, the agreement, in general, is within experimental error.

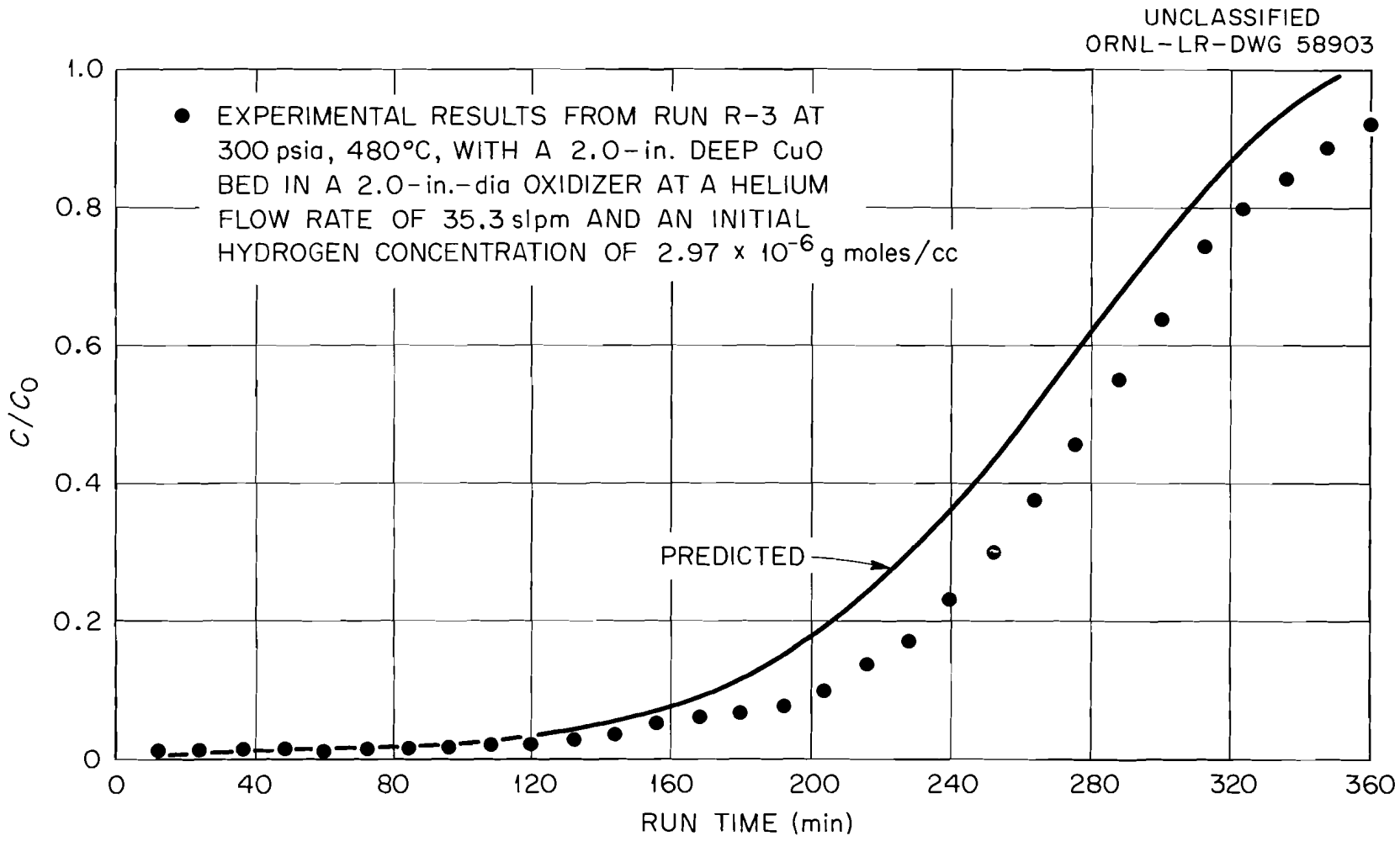

Fig. 1.1. Comparison between experimental results from run R-3 and predicted results from the mathematical model of external diffusion and internal diffusion controlling a rapid, irreversible reaction of hydrogen with porous pellets of CuO.

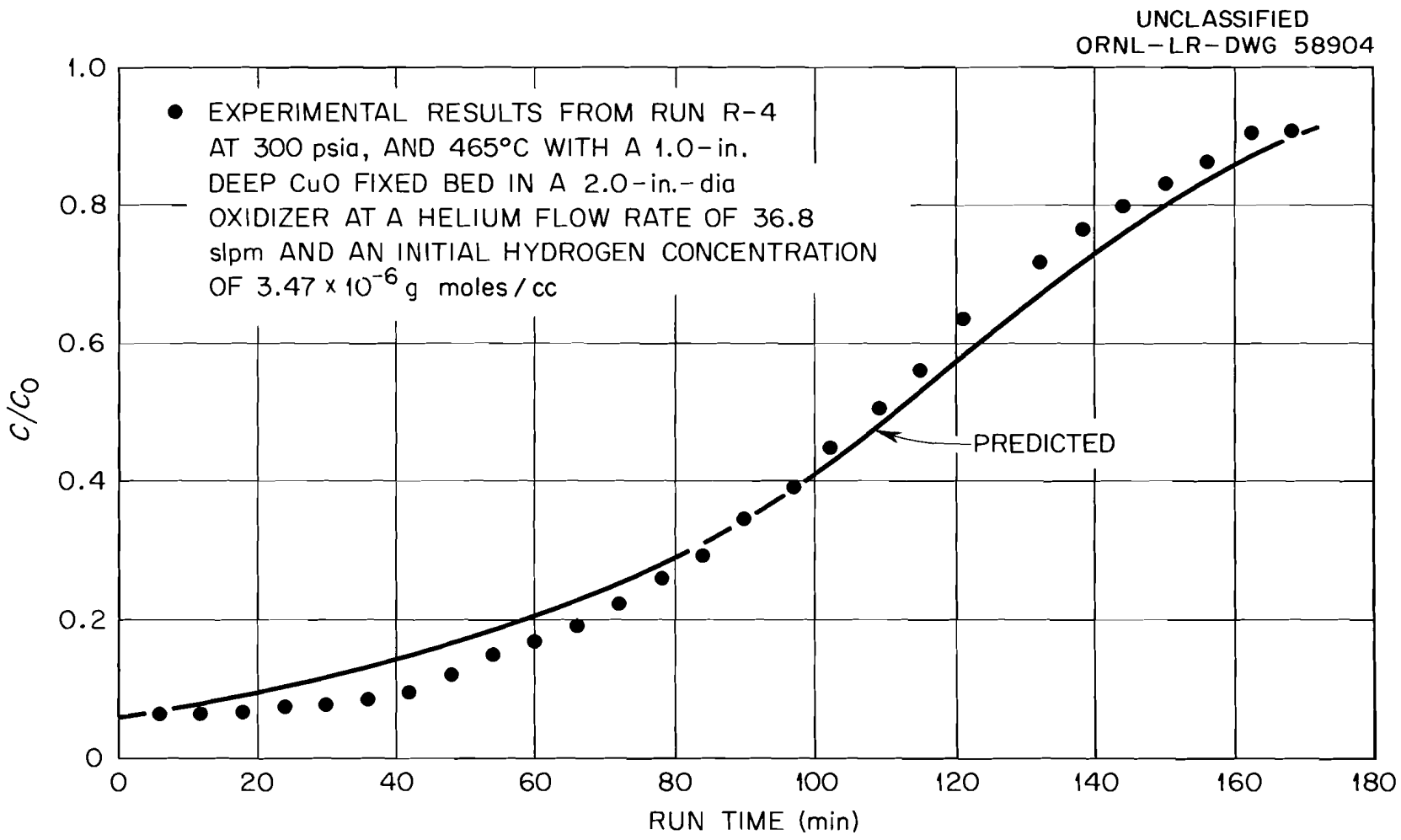

Fig. 1.2. Comparison between experimental results from run R-4 and predicted results from the mathematical model of external diffusion and internal diffusion of hydrogen controlling a rapid, irreversible reaction of hydrogen with porous pellets of CuO.

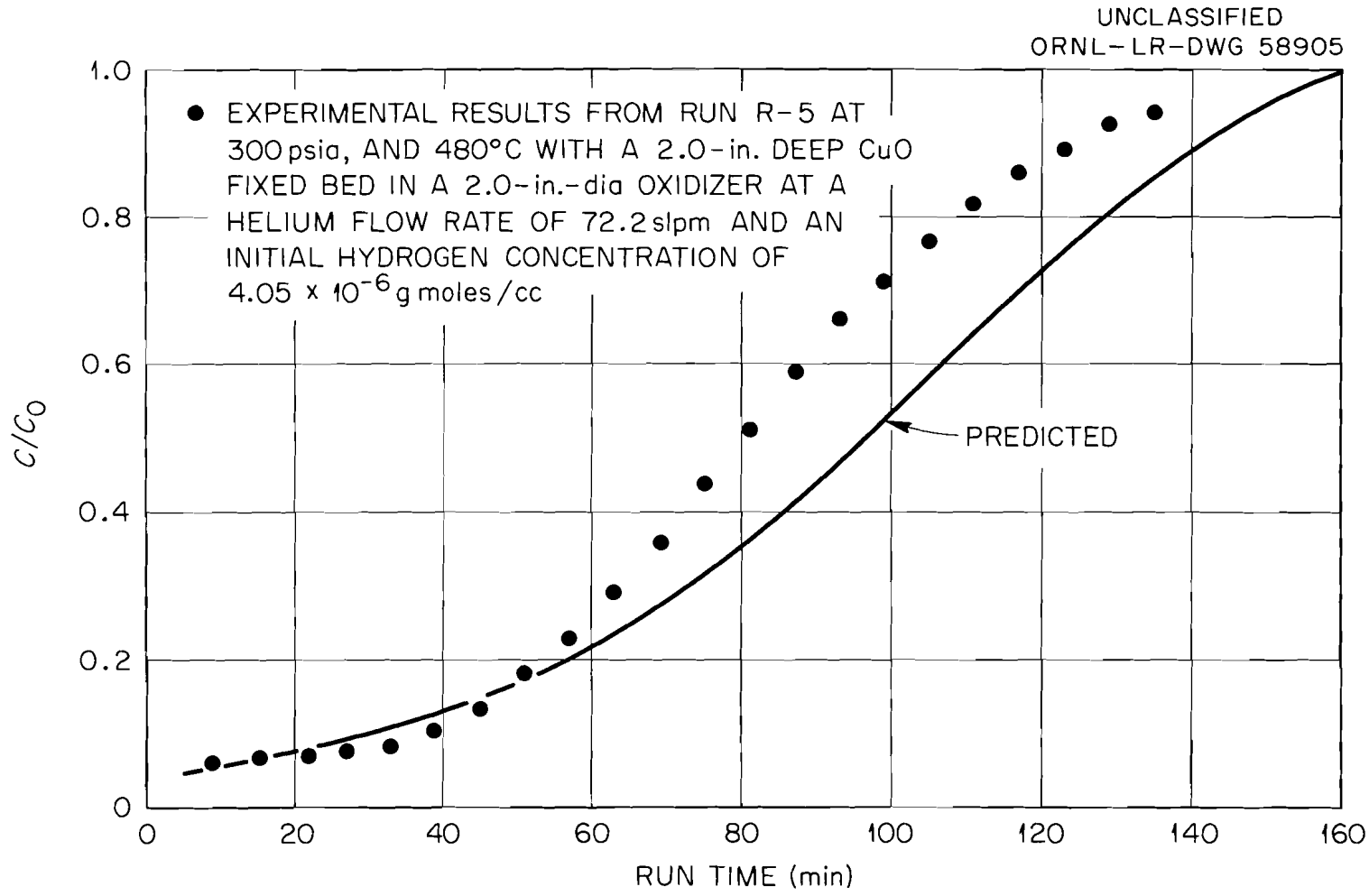

Fig. 1.3. Comparison between experimental results from run R-5 and predicted results from the mathematical model of external diffusion and internal diffusion of hydrogen controlling a rapid, irreversible reaction of hydrogen with porous pellets of CuO.

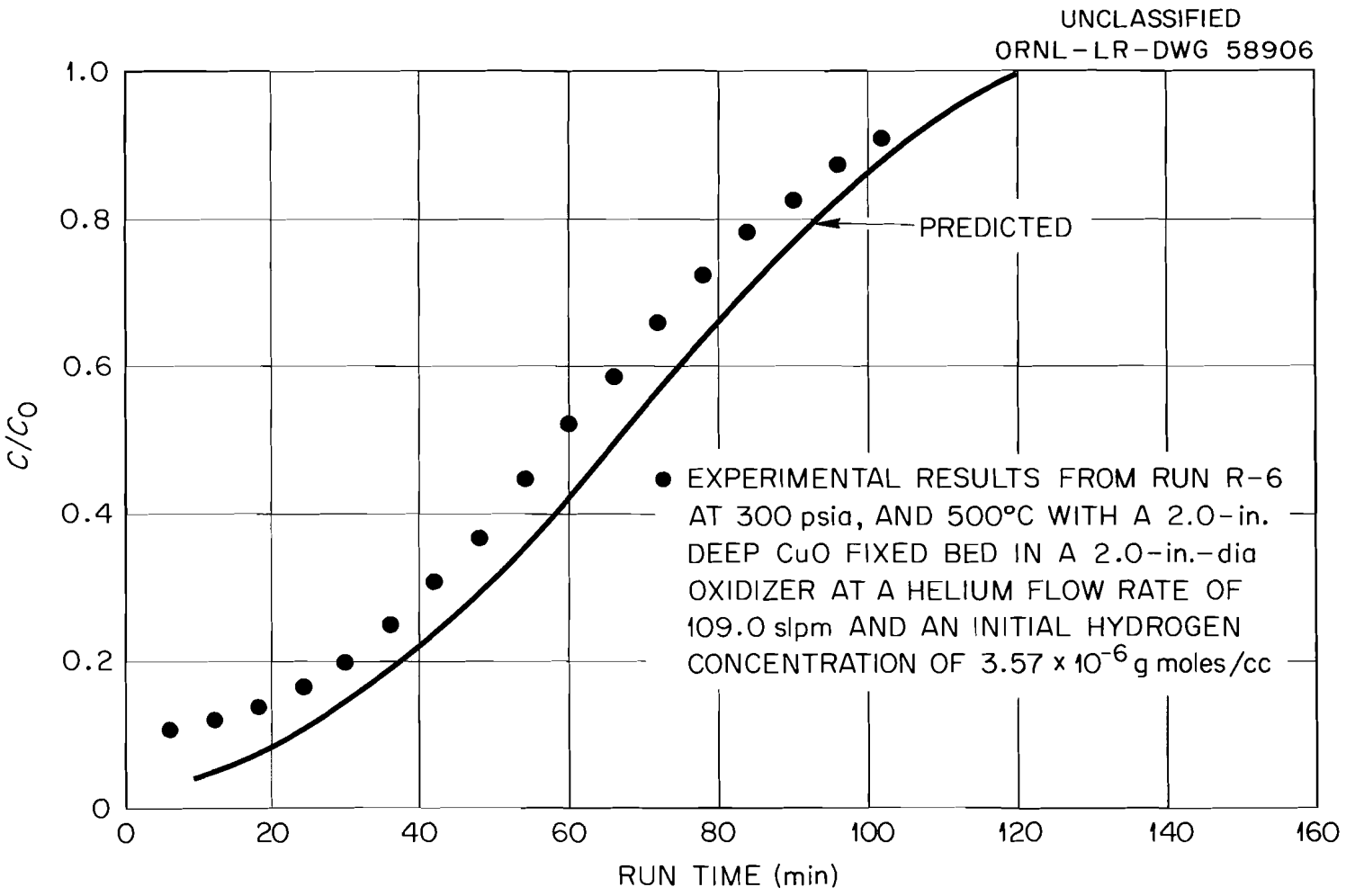

Fig. 1.4. Comparison between experimental results from run R-6 and predicted results from the mathematical model of external diffusion and internal diffusion of hydrogen controlling a rapid, irreversible reaction of hydrogen with porous pellets of CuO.

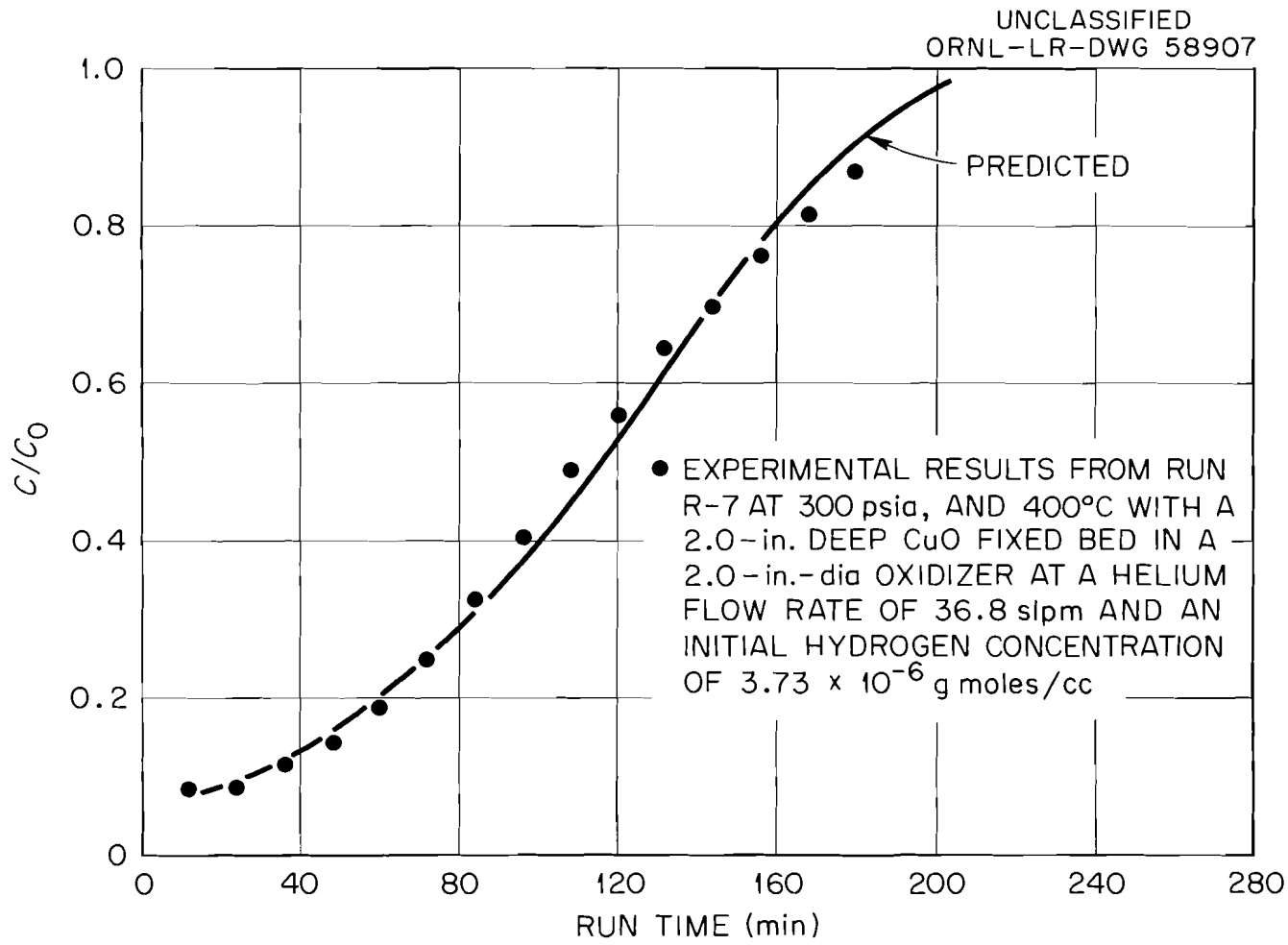

Fig. 1.5. Comparison between experimental results from run R-7 and predicted results from the mathematical model of external diffusion and internal diffusion of hydrogen controlling a rapid, irreversible reaction of hydrogen with porous pellets of CuO.

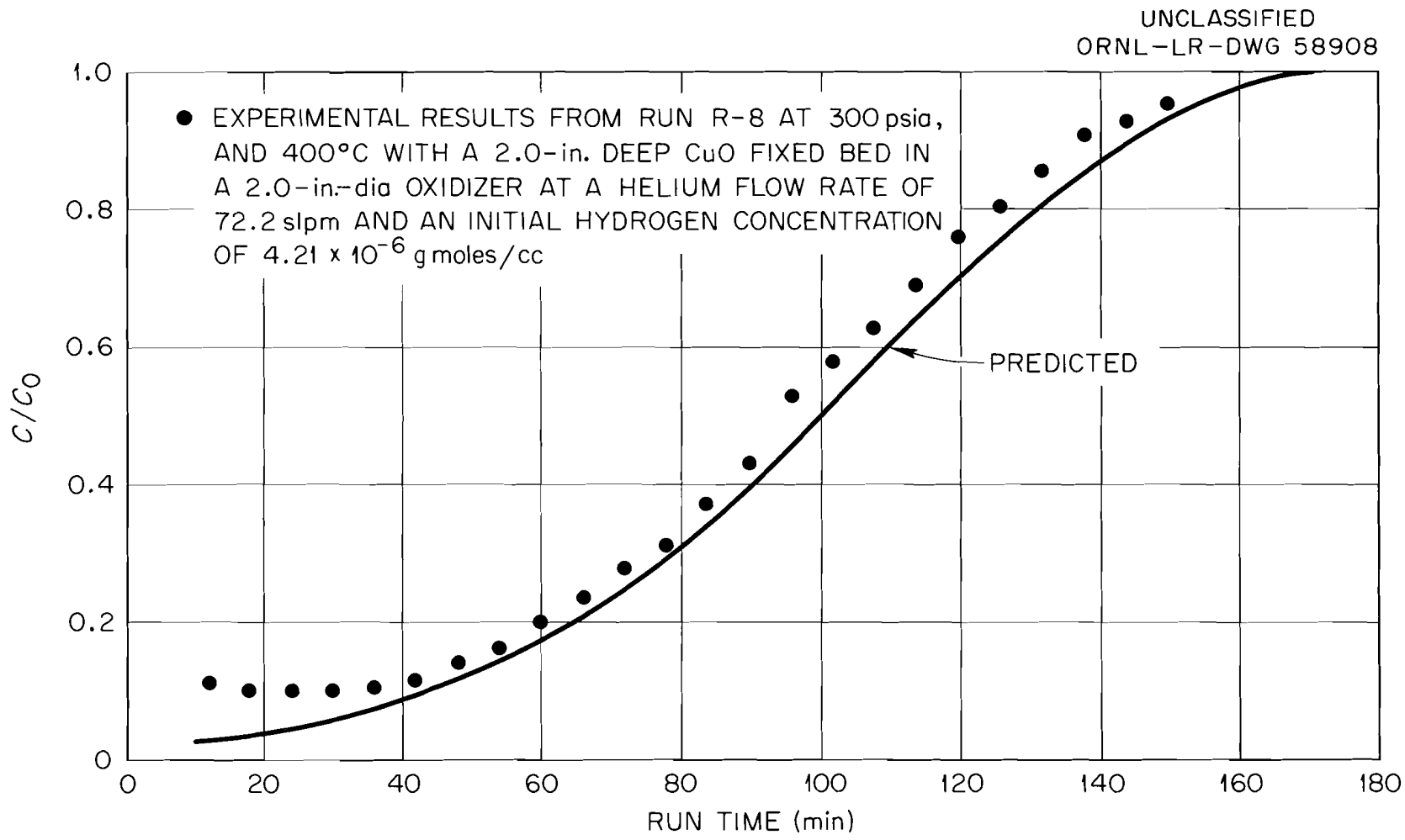

Fig. 1.6. Comparison between experimental results from run R-8 and predicted results from the mathematical model of external diffusion and internal diffusion of hydrogen controlling a rapid, irreversible reaction of hydrogen with porous pellets of CuO.

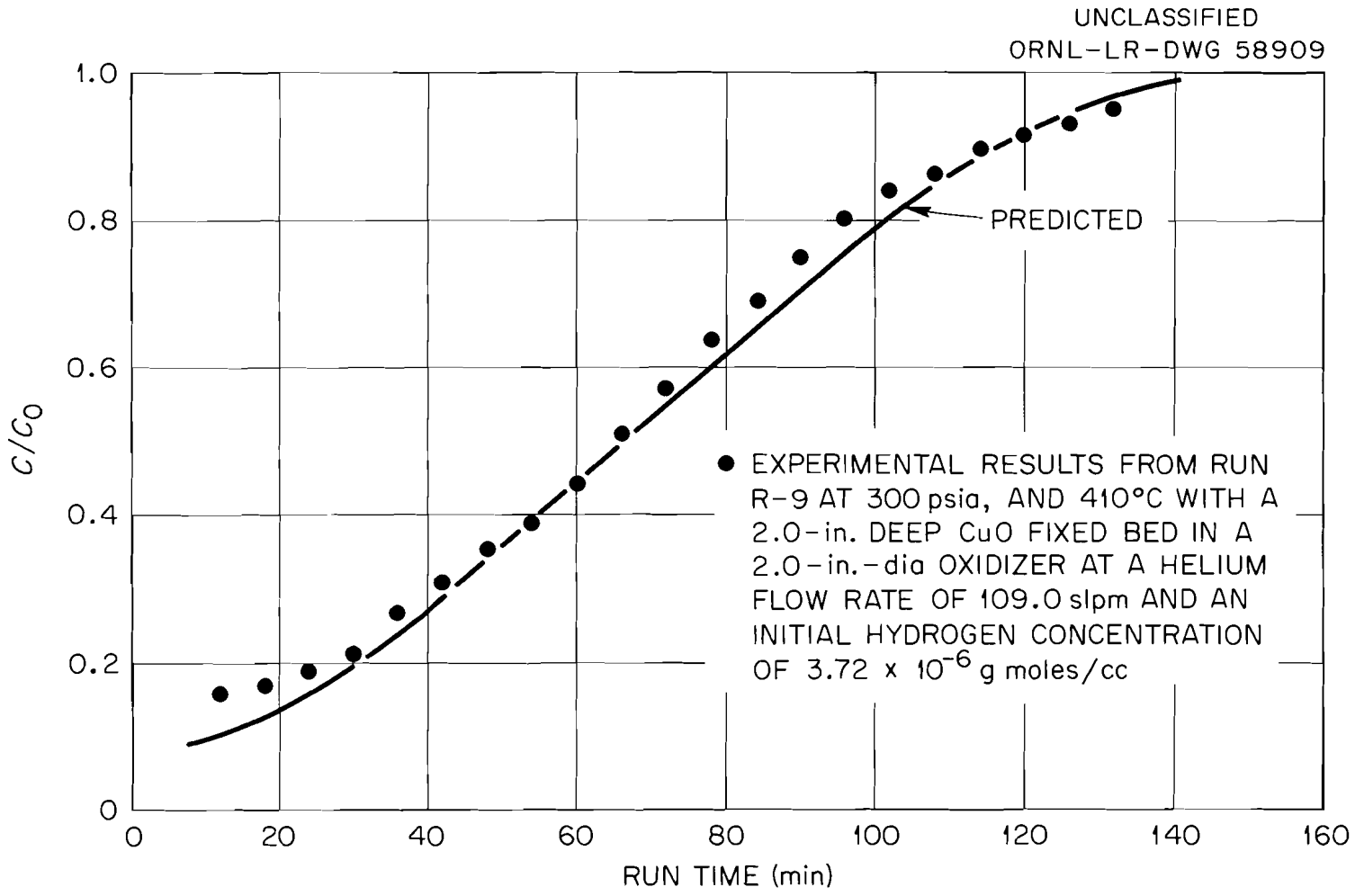

Fig. 1.7. Comparison between experimental results from run R-9 and predicted results from the mathematical model of external diffusion and internal diffusion of hydrogen controlling a rapid, irreversible reaction of hydrogen with porous pellets of CuO.

2.0 ION EXCHANGE

J. C. Suddath

2.1 Predictions of Uranyl Sulfate Loading Rates on Chloride Equilibrated Dowex 21K - J. S. Watson

In recent months predicted uranyl sulfate loading rates on chloride equilibrated resin have been shown to be a function of the equilibrium sulfate to uranyl sulfate loading on the resin. Exact measurements of this ratio experimentally has not been possible, but an assumed value of approximately 0.02 in the calculations has been shown to give good agreement between measured and predicted loading rates with 960 micron Dowex 21K and a loading solution 0.005 M in uranyl sulfate and 0.020 M in sulfuric acid. This value of the ratio also allows reasonably accurate predictions of the rate at which chloride ions leave the resin during the uranyl sulfate loading.

The most recent efforts have been directed toward determining if this same behavior is found with other resin samples, and to determine if the loading rate is a function of the loading solution uranium or sulfate concentrations. Loading runs have been made with a 0.006 M uranyl sulfate solution. The total sulfate concentration of the solution was varied from 0.026 M to 0.201 M in total sulfate by adding sodium sulfate between runs. A run was also made with a 0.003 M uranyl sulfate solution 0.11 M in total sulfate. Both solutions were 0.020 M in sulfuric acid. The results of these runs are shown in Figure 2.1. Over this concentration there were no significant variations in the loading rate. According to the proposed model, this implies that no significant variation in the equilibrium sulfate to uranyl sulfate loading occures.

Calculations and experimental measurements of the rate of chloride loss from 820 micron resin during uranyl sulfate loading have been made. The results (Figure 2.2) show that good agreement between the predicted and measured loss rates are obtained if one assumes that the equilibrium sulfate to uranyl sulfate loading ratio is 0.02. This is identical to the results obtained with 960 micron resin.

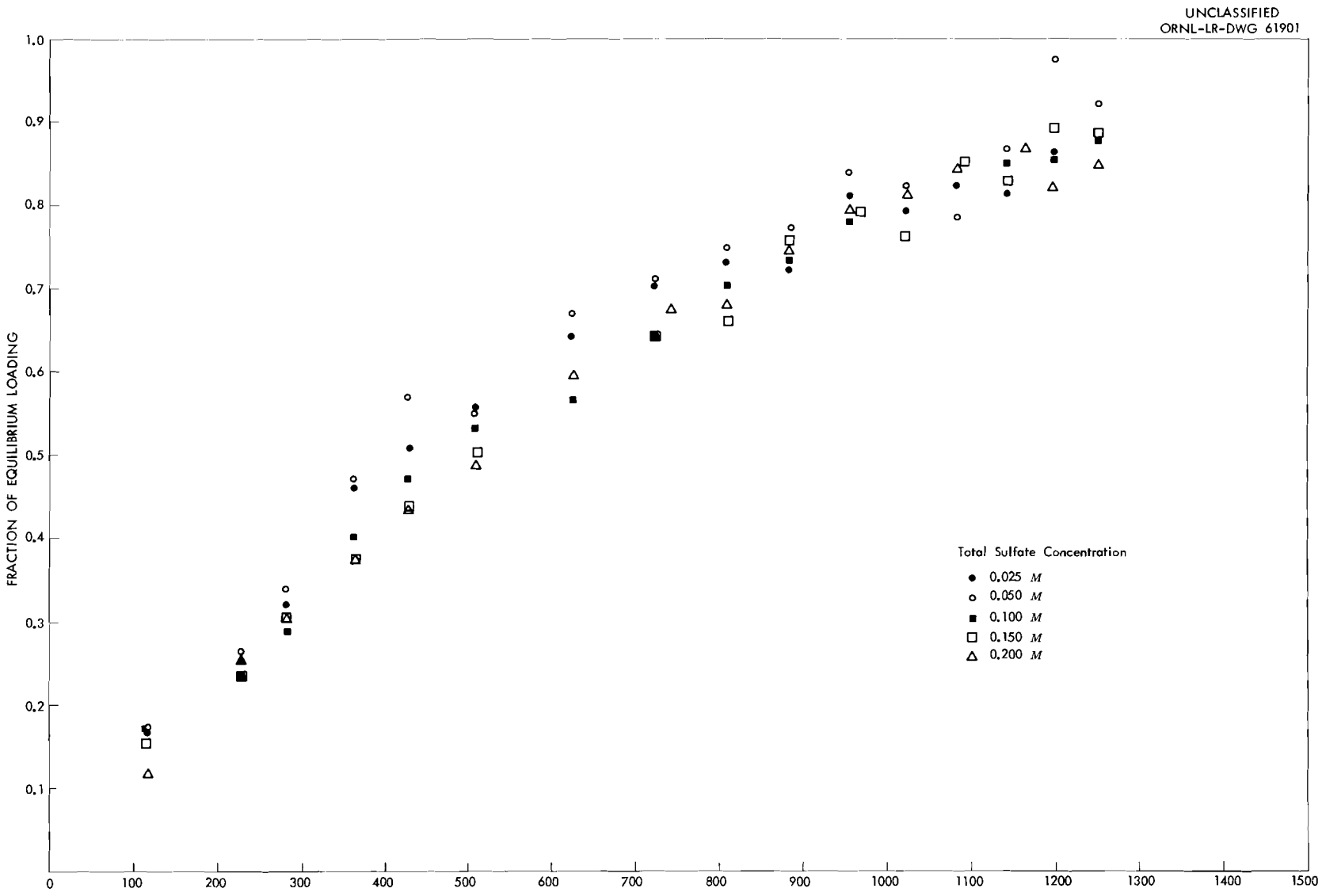

Fig. 2.1. The rate of uranyl sulfate loading on chloride equilibrated 960 micron Dowex 21 K.

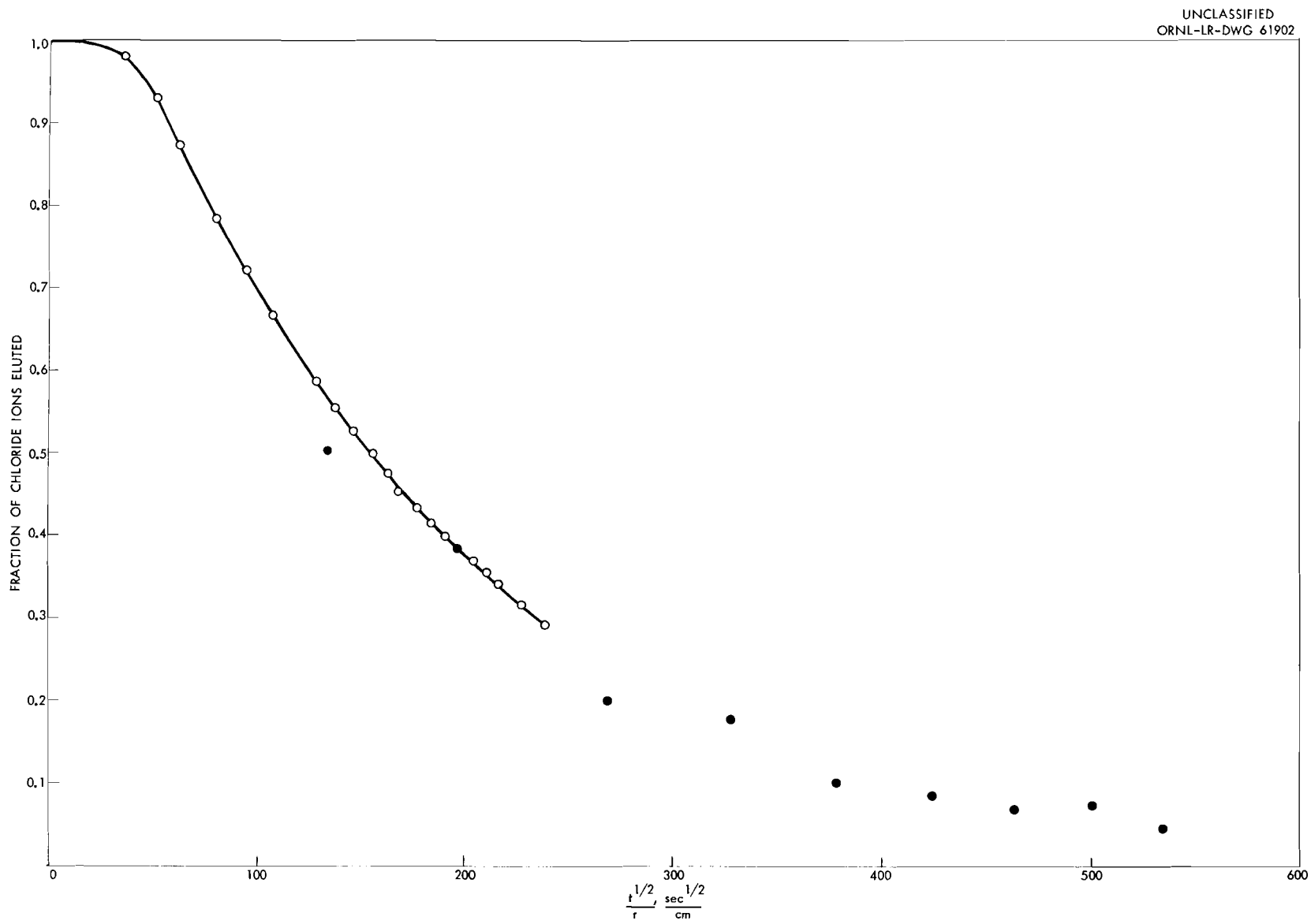

Fig. 2.2. The rate of chloride loss from 820 micron Dowex 21 K during uranyl sulfate loading.

3.0 POWER REACTOR FUEL PROCESSING

C. D. Watson

3.1 U-C Fuel Processing - B. A. Hannaford

Proposed reactor fuels of the uranium-graphite type contain particulate compounds (UO_2, UO_2-ThO_2, UC_2, UC_2-ThC_2) dispersed in a graphite matrix. Fuel particles may be uncoated or coated with a refractory (Al_2O_3, pyrolytic carbon); fuel elements may be coated with SiC or associated with unfueled graphite.

As the basis for a preliminary estimate of the cost of processing a uranium graphite fuel, a continuously-loaded 350 MWT Pebble Bed Reactor was chosen. Processing load, assuming plant operation 300 days per year, would be 100 kg/day. Fuel was assumed to be UC_2-ThC_2 particles coated with pyrolytic carbon, dispersed in 1-1/2-in. spheres covered with Si-SiC.

Figure 3.1 represents an untried semi-continuous flowsheet, contrived primarily as a basis for the preliminary cost estimate. The dissolver is an upright slab designed for moderate (1 to 2 atm) gas overpressure to drive fuming HNO_3 and wash water through the deep bed of disintegrated graphite and the supporting sand filter. A small gas stream is continuously bled off to the condenser and off-gas treatment system. Following an initial soak period, during which the cracked spheres are largely disintegrated, continuous flow of acid through the dissolver is begun. Boil-down of acid leach solution prior to mixing with wash water would permit recycle of the bulk of fuming HNO_3. Leached graphite, SiC, and sand would be fluidized and/or jetted to waste.

A make-up volume of 115 liter of 22.5 M HNO_3 would be required for the succeeding 100 kg batch of fuel, dictated primarily by the size of the waste acid cut during boil-down. Stoichiometry of the reaction of UC_2, ThC_2 with fuming HNO_3 is not known; however, acid consumption due to chemical reaction and thermal decomposition would be small in comparison with the loss to waste acid overhead. An acid concentration of 22.5 M (95%) was chosen in order that acid in the dissolver would not drop below ~21.2 M. Volume and compositions of virtually all streams shown - acid dissolvent, water wash, recycle acid, waste acid, and off-gas - are highly tentative, and require experimental verification.

3.2 Modified Zirflex - F. G. Kitts

Modified Zirflex denotes a process for the recovery of uranium from U-Zr-Sn fuels by batchwise dissolution in NH_4F-NH_4NO_3-H_2O_2 solutions, stabilization with HNO_3-$Al(NO_3)_3$, and TBP extraction. During dissolution a small, continuous addition of hydrogen peroxide is made to oxidize U^{IV} to the more soluble U^{VI}. Such a process is desirable for processing zirconium fuels containing higher per centages of U (up to 10%) without the intermediate precipitation of UF_4 which would occur if no oxidant were added. Presently dissolutions of unirradiated zirconium fuels are being carried out both on a laboratory scale and in engineering-scale equipment.

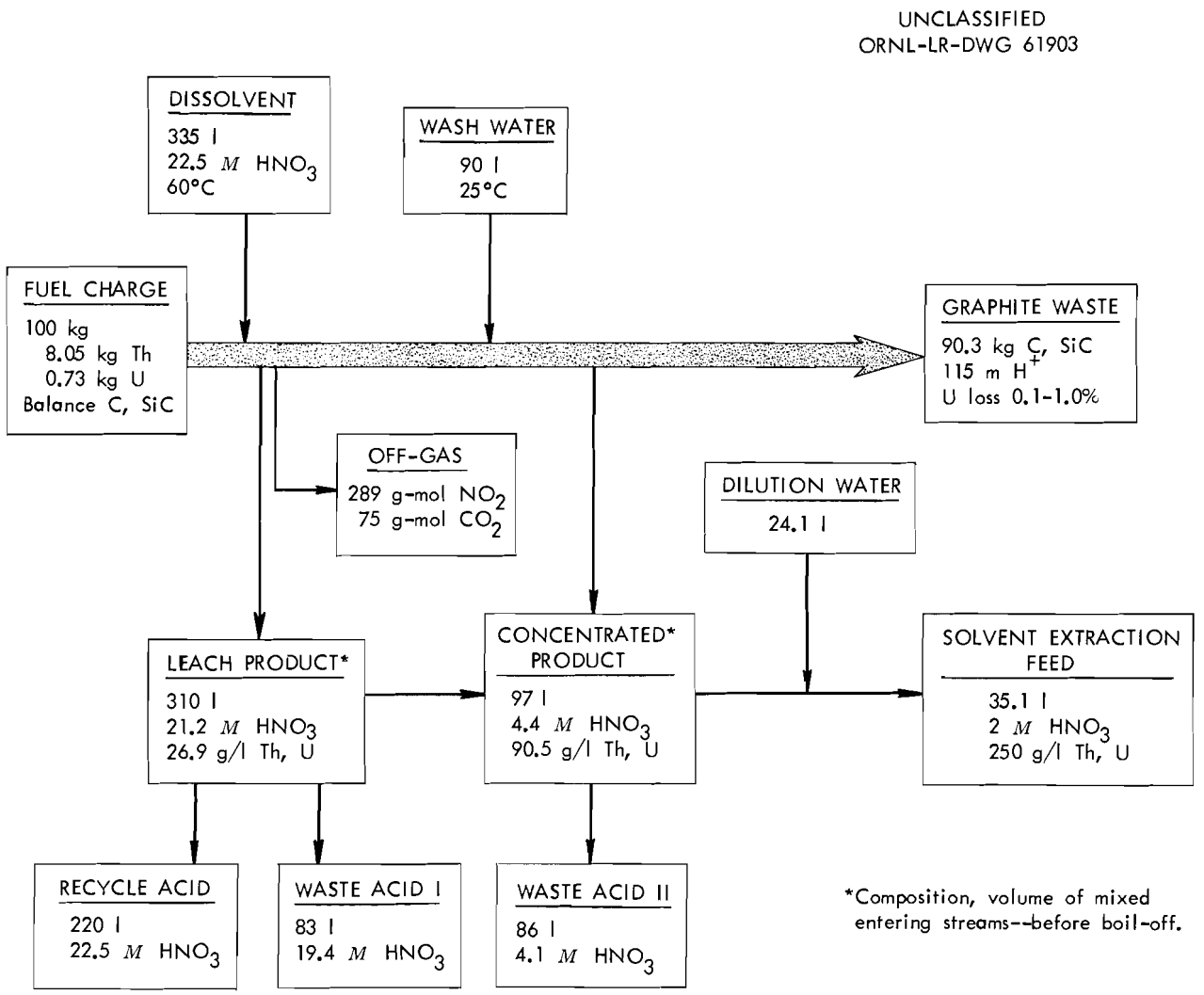

Fig. 3.1. Tentative flow sheet for processing PBR fuel containing ThC_2, UC_2, in 22.5 M HNO_3.

Run CZr-5 was made in the engineering-scale equipment using dissolvent initially 6.53 M NH_4F-0.00 M NH_4NO_3-0.01 M H_2O_2 and a H_2O_2 addition rate of 0.5×10^{-5} mols/cm^2-min (Table 3.1). The 1.103 kg of unoxidized 8% U-Zr plate (0.122 in. thick) was completely dissolved in 2 hrs of refluxing. About 4 g of a green precipitate was collected which contained 56% U, 25% F and 3% Zr. It is assumed that this is the same material involved in the coat formation reported by Gens (ORNL-2905) since the free fluoride to U ratio was only 51. The amounts of gaseous reaction products evolved agreed very well with the assumed stoichiometry of the dissolution reaction with 2.0 moles of H_2 and 4.2 moles of NH_3 observed per mole of Zr dissolved. Four samples of the scrubbed off-gas taken at intervals throughout the run showed $H_2 \geqq 93\%$ with $H_2 + H_2O \cong 99\%$ and $O_2 \leqq 0.15\%$. The average boil-up rate (obtained by measuring the reflux to the dissolver) was 0.15 ml/min-cm^2 of initial fuel surface. The addition of stabilizer [1.8 M HNO_3 - 1.8 M $Al(NO_3)_3$] at room temperature when the dissolution product had cooled to ~90°C produced a stable solvent extraction feed containing 0.35 M Zr, 2.78 g U/liter, 2.7 M F, 1 M HNO_3 and 1 M $Al(NO_3)_3$. Material balances for Zr, U and F accounted for 93.5 - 95.5% of the total amount of each element charged.

Runs MZr-17, 18 and 19 were made in the 1-in.-dia recirculating dissolver to learn the effect on dissolution of a different strength (6%) and method of H_2O_2 addition. The volumetric addition rate was maintained the same as with 3% solution resulting in an approximate doubling of the molar rate. No change in dissolution rate was observed but the solutions turned yellow earlier indicating a lower U^{IV} concentration in the middle stages of dissolution. The HNO_3-$Al(NO_3)_3$ stabilized portion of MZr-17 was a stable solution (Table 3.1). Neither solution in MZr-19 (also HNO_3-$Al(NO_3)_3$ stabilized) was stable for thirty days; the first portion [0.8 M HNO_3-$Al(NO_3)_3$] produced white crystals while the second [1.0 M HNO_3-$Al(NO_3)_3$] produced a suspended gelatinous precipitate. All three of the H_2O stabilized solutions were stable; the most highly loaded one contained 0.444 M Zr, 3.28 M F and 3.54 g U/liter.

Run CZr-6 (Table 3.1) was the dissolution of a TRIGA "meat" slug (8% U-ZrH, ~1.4 in. ø x 14 in. long). The large diameter (~1.4 in.) of the slug resulted in a low area to mass ratio and a long dissolution time. This necessitated high H_2O_2 addition and boil-up rates, on an area basis, in order to give streams of the desired magnitude. The H_2O_2 volumetric rate was still low (2 - 6 cc/min) so that considerable gassing (indicating H_2O_2 decomposition) was observed at the inlet to the dissolver. Although the NH_3 evolution rate and O_2 percentage are believed reliable, the $H_2 + O_2 + (N_2?)$ evolution rate (Figure 3.2) is in error (low) due to a malfunction in the scrubbed off-gas metering system.

The 8% U-ZrH slug dissolution described above was only one step in the processing (Figure 3.2) of a genuine TRIGA element. The removal of the 0.030 in. Al clad and dissolution of the Al-Sm poison discs were accomplished in less than 1/2 hr at reflux in an excess of 2 M NaOH-1.8 M $NaNO_3$ (the large volume of dissolvent was required to cover the 28-in. long element in The 6-in.-dia dissolver). The soluble U loss was 0.015% with about an equal amount carried by a gelatinous precipitate [presumed $Fe(OH)_3$]. After

Table 3.1. Data for Modified Zirflex Runs

Run No.	Dissolvent Vol ml	Dissolvent NH_4F M	Dissolvent NH_4NO_3 M	Dissolvent H_2O_2 M	U-Zr-Sn Type	U-Zr-Sn Wt g	U-Zr-Sn Diss. %	U-Zr-Sn Area cm^2	H_2O_2 Add Rate moles/cm^2-min	Diss. Time hours	H_2/Zr mols	NH_3/Zr mols	Scrubbed Off-gas Vol ft^3	Scrubbed Off-gas $H_2 + H_2O$ %	Scrubbed Off-gas O_2 %	Boil-up Rate ml/cm^2-min	NH_4OH in Reflux M
CZr-5	13,350	6.53	0.00	0.01	8% U-Zr	1103	100	1077	0.5×10^{-5}	2.0	2.0	4.2	18.2	99	0.1	0.15	0.6-0.1
CZr-6	27,514	6.3	0.6	0.01	TRIGA	2274	99-3/4	412	1.6×10^{-5}	11.5	-	5.3	-	-	>10	0.4	0.6-0.1
MZr-17	254[a]	6.53	0.00	0.01	8% U-Zr	21.00	100	23	1.3×10^{-5}	1.9	-	-	-	-	-	-	-
MZr-18	241[a]	6.53	0.00	0.01	8% U-Zr	20.32	100	23	1.1×10^{-5}	2.0	-	-	-	-	-	-	-
MZr-19	245[a]	6.58	0.00	0.01	TRIGA	20.94	100	14.2	1.1×10^{-5}	3.75	-	-	-	-	-	-	-

Run No.	Stabilizer Vol ml	Stabilizer HNO_3 M	Stabilizer $Al(NO_3)_3$ M	Solvent Extraction Feed Vol ml	Zr g/ℓ	U g/ℓ	F M	HNO_3 M	Al^{+3} M	Material Balances Zr %	U %	F %
CZr-5	17,000	1.8	1.8	30.3	31.9	2.78	2.7	1.0	1.0	95.2	95.4	93.7
CZr-6	21,600	1.8	1.8	49.95	39.2	3.31	3.3	0.78	0.78	94.4	93.8	94.2
MZr-17	155	1.8	1.8	266	33.9	2.92	3.0	1.05	1.05	95.2	94.8	97.5
	200[b]	0.0	0.0	323	29.0	2.53	2.54	0.0	0.0			
MZr-18	108[b]	0.0	0.0	226	40.5	3.54	3.28	0.0	0.0	97.9	97.9	94.9
	145[b]	0.0	0.0	263	34.8	3.01	2.85	0.0	0.0			
MZr-19	96	1.8	1.8	216	41.8	3.44	3.53	0.80	0.80	94.5	88.8	91.9
	150	1.8	1.8	270	33.4	2.76	2.66	1.0	1.0			

[a] After dissolution, the batch was split into two equal volumes and stabilized as indicated.

[b] H_2O

UNCLASSIFIED
ORNL-LR-DWG 58791

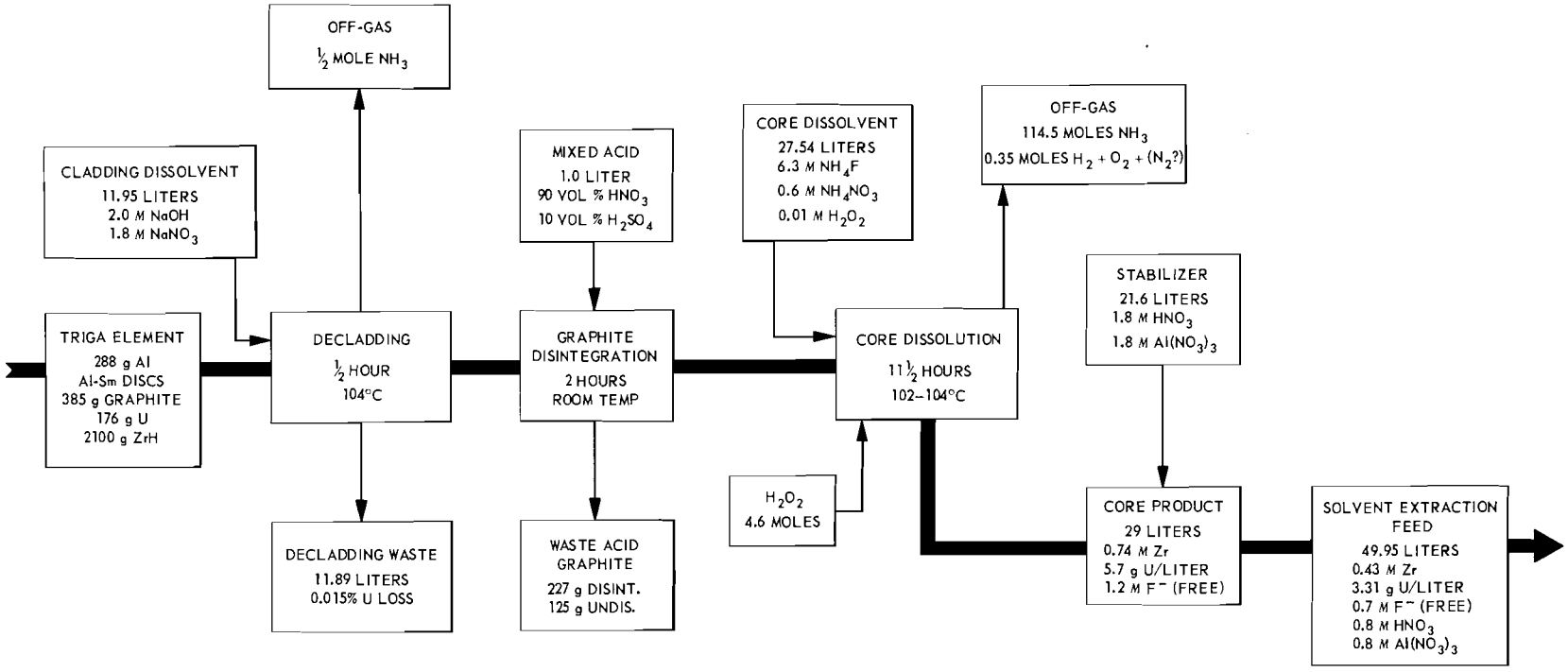

Aqueous Processing of Triga Fuel.

Fig. 3.2. Aqueous processing of TRIGA fuel.

thorough washing and drying 1.0 liter of 90 vol % WFNA - 10 vol % H_2SO_4 (fuming) was admitted to the dissolver for disintegration of the two ~1.4-in.-dia x 4-in. long graphite slugs. After 2 hrs exposure at room temperature the graphite was 2/3 (by wt) disintegrated (equal attack on both pieces). Due to the system geometry the U-ZrH slug was not subjected to the acid mixture; low U losses were reported by Gens (ORNL-3065). The Al end pieces were only slightly attacked.

It is believed that future investigation should include a preliminary mechanical preparation which would require only the cutting of the 0.030 in. Al cylinder near each end of the U-ZrH slug. This would eliminate the graphite slugs, the Sm poison discs and the massive Al end fittings from the dissolution cycle. Even if the U-ZrH slug could not be mechanically separated from its Al tube the process would be reduced to a much simpler two step operation with the elimination of the hazards of handling fuming HNO_3-H_2SO_4, exhaustive washings and the removal of Al heels and granular graphite from the dissolver.

3.3 Shearing and Leaching - B. C. Finney

A chop and leach program to determine the economic and technological feasibility of continuously leaching the core material (UO_2 or UO_2-ThO_2) from relatively short sections (1-in. long) of fuel elements produced by shearing is continuing. This processing method enjoys the apparent advantage of recovering fissile and fertile material from spent power reactor fuel elements without dissolution of the inert jacketing material and end adapters. These unfueled portions are stored directly in a minimum volume as solid waste. A "cold" chop-leach complex consisting of a shear, conveyor, leacher, and compactor is being evaluated prior to "hot" runs.

Leaching. Three dissolution runs were made in the glassware leacher model (Table 3.2) and in each run 9 batches of UO_2 pellets (whole unirradiated PWR rejects) were dissolved with a program to simulate 4 stages. In the first run (run 25), 4 M HNO_3 was used as dissolvent at a HNO_3/UO_2 mole ratio of 5.4; this resulted in slightly less than complete dissolution of the UO_2 (98.4 - 99.4%) in a 4 hr dissolution time.

Two runs were made using 8 M HNO_3 as the dissolvent. The first (run 26) was made at a HNO_3/UO_2 mole ratio of 4. The instantaneous uranium loading and acidity as a function of dissolution time are presented in Figure 3.3. The uranium loading varied from a maximum of ~600 g/liter to a minimum of 350 g/liter while the acidity varied from a minimum of 1.1 M HNO_3 to a maximum of 3.6 M HNO_3. Steady state was attained in approximately 3 batches and the composite product at apparent steady state as represented by the portion of the curves above line AB was ~500 g U/liter and 1.9 M HNO_3.

Run 27 was made at a HNO_3/UO_2 mole ratio of 6.15 (Figure 3.4). Again steady state was attained in approximately 3 batches of UO_2. With exception of the 6th batch, the maximum uranium loading varied from 375-425 g/liter to a minimum of approximately 200 g/liter and the acidity varied from a maximum of approximately 6 M HNO_3 to a minimum of approximately 2.7 M HNO_3.

Table 3.2. Leacher Model Dissolution Data UO_2-HNO_3 System

Pellets: PWR Rejects (0.370-in.-OD x 0.390-in. long, edges chipped) $\rho \cong 10.3$ g/cc

Run No.	UO_2 Batches Used	Dissolution Time min	Temp. °C	Dissolvent (HNO_3) M	Dissolvent (HNO_3) Flow Rate ml/min	Dissolvent (HNO_3) Vol liters	UO_2 Pellets Wt Charged g	UO_2 Pellets % Dissolved	Product (Composite) Loading g U/liter	Product (Composite) H^+ M	Product (Composite) Vol liters	Off-gas Nitrogen g-mol	Off-gas % of HNO_3 Feed	Acid Composition g-mol NO_3^- / g-mol U
25	No. 1	240	100-104	4	50.2	33.6	599.7	99.4	130	2.58	36.6	10	6.9	2.49
	No. 2	240	101-103				601.3	98.5						
	No. 3	240	101-102				601.0	98.4						
	No. 4	240	100-102				603.2	98.8						
	No. 5	240	100-103				600.3	99.0						
	No. 6	240	100-102				600.0	98.9						
	No. 7	240	101-103				600.0	99.3						
	No. 8	240	100-102				600.0	99.0						
	No. 9	240	101-103				604.4	99.1						
26	No. 1	240	102-110	8	18.6	12.3	601.4	100	393	3.61	12.1	10.6	10.75	2.46
	No. 2	240	102-107				601.5	100						
	No. 3	240	102-106				600.5	100						
	No. 4	240	102-104				600.6	100						
	No. 5	240	101-107				601.4	100						
	No. 6	240	102-108				600.7	100						
	No. 7	240	101-107				601.2	100						
	No. 8	240	101-105				601.2	100						
	No. 9	240	102-105				600.4	100						
27	No. 1	240	100-110	8	28.5	18.8	600.0	100	254	5.25	18.7	12	8	2.60
	No. 2	240	101-111				601.0	100						
	No. 3	240	100-110				600.0	100						
	No. 4	240	101-110				600.2	100						
	No. 5	240	102-110				600.1	100						
	No. 6	240	102-111				600.7	100						
	No. 7	240	101-110				600.0	100						
	No. 8	240	103-110				600.0	100						
	No. 9	240	102-110				600.0	100						

UNCLASSIFIED
ORNL-LR-DWG 61904

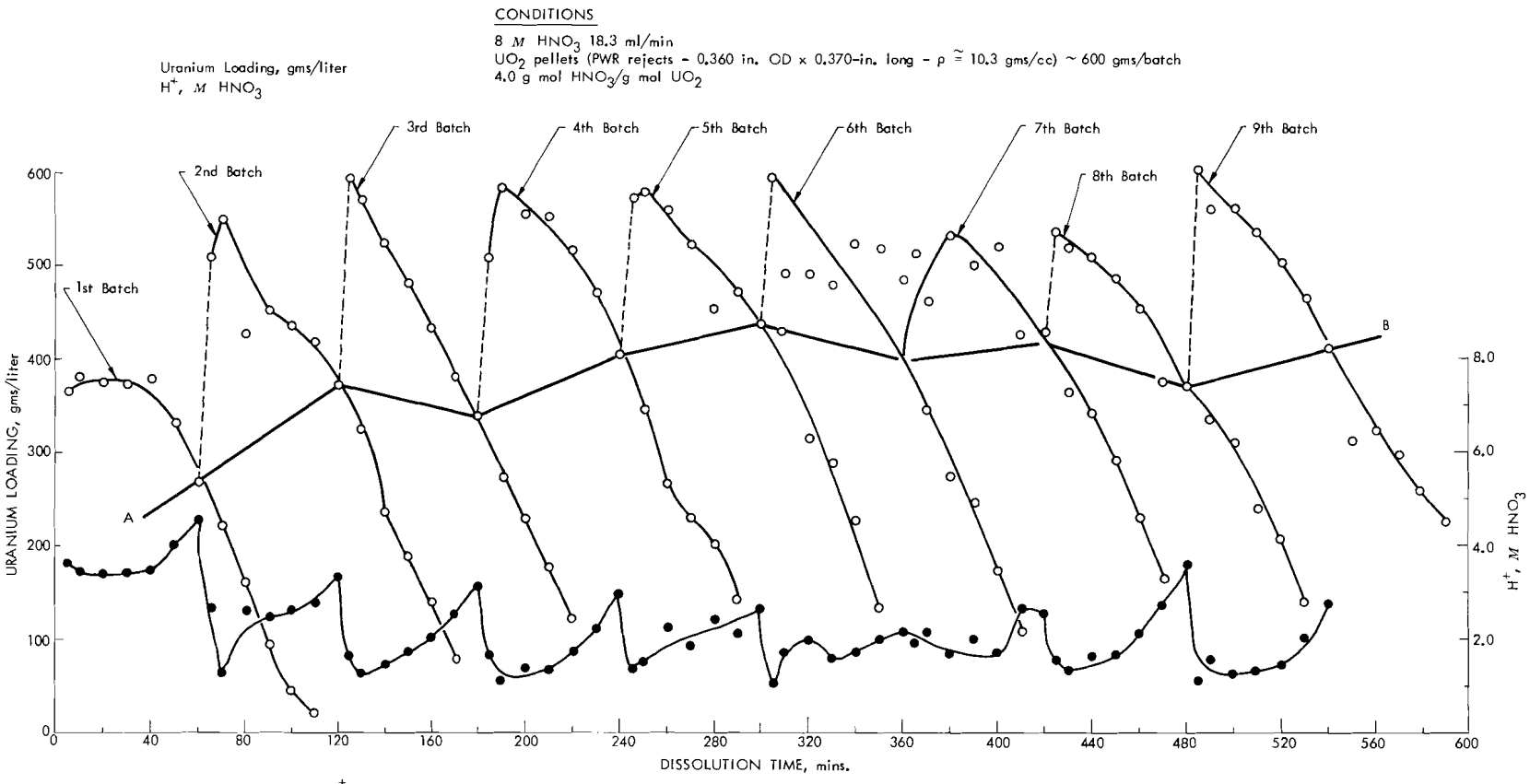

Fig. 3.3. Uranium loading and H^+ as a function of dissolution time for the dissolution of nine batches of UO_2 pellets (Run-26) in the four stage leacher model based on a four hour dissolution time per batch.

UNCLASSIFIED
ORNL-LR-DWG 61905

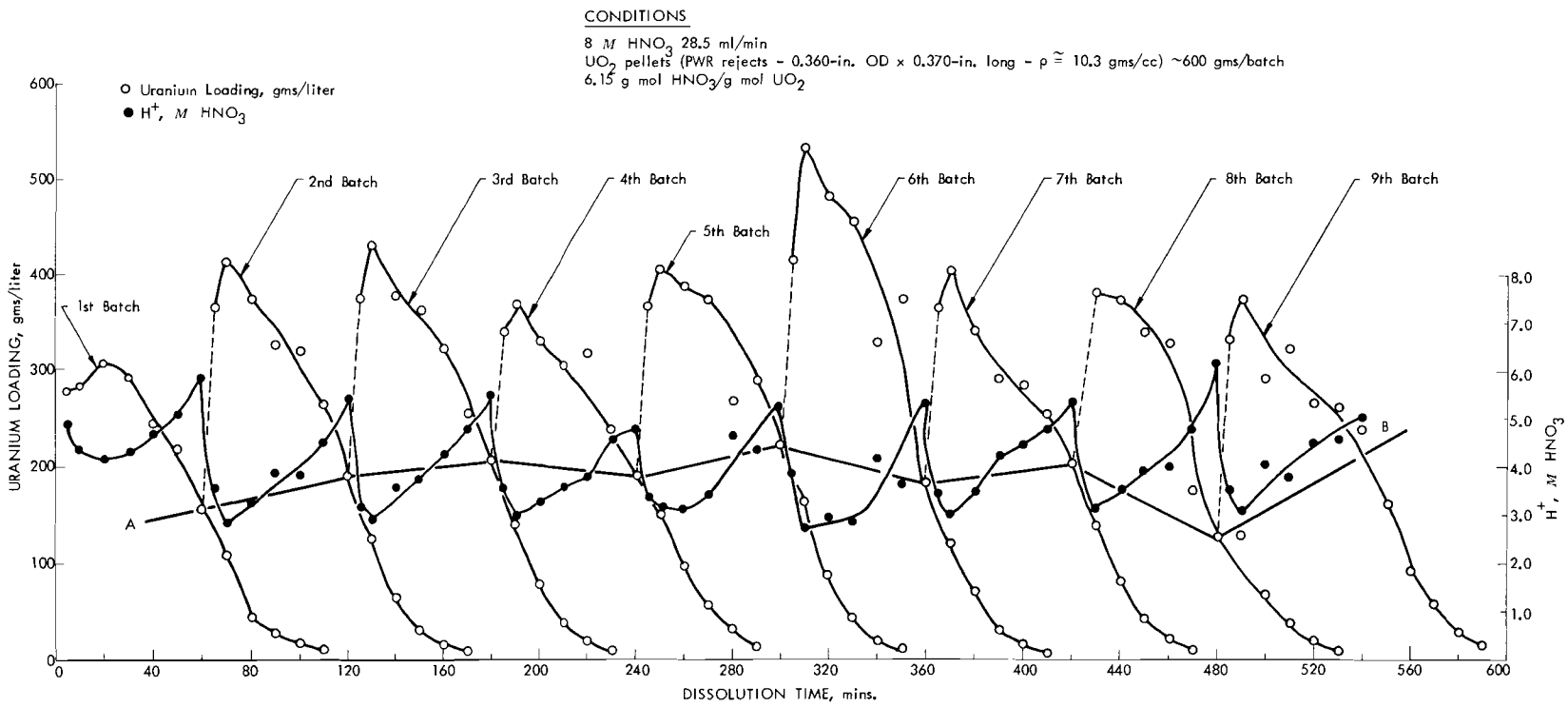

Fig. 3.4. Uranium loading and H^+ as a function of dissolution time for the dissolution of nine batches of UO_2 pellets (Run-27) in the four stage leacher model based on a four hour dissolution time per batch.

The composite product at apparent steady state was 325-350 g U/liter and approximately 4 M HNO_3. In comparing runs 26 and 27 a 50% increase in the HNO_3/UO_2 mole ratio resulted in approximately a 30% decrease in the composite product uranium loading and approximately a 100% increase in the composite product acidity.

4.0 SOLVENT EXTRACTION STUDIES

A. D. Ryon

The flooding rates and holdup data reported this month were obtained using the 5% TBP-1.8 M $Al(NO_3)_3$ flowsheet. The experimental techniques and a description of the columns may be found in the October 1959 Unit Operations monthly report (CF 59-10-77).

4.1 Flooding Rate Studies - R. S. Lowrie, F. L. Daley

Studies were made to determine the flooding rates for aqueous continuous operation of sieve plate (0.125-in.-dia holes, 23% free area) pulse columns under conditions similar to the 5% TBP-1.8 M $Al(NO_3)_3$ flowsheet. Physical properties of the solvent and aqueous feeds are shown in Table 4.1. Flooding rates for aqueous continuous operation of the 24 ft compound extraction scrub column where mass transfer of uranium occurred increased from 580 to 2010 gal-ft^{-2}hr^{-1} as the pulse frequency decreased from 90 to 50 cpm (Table 4.2). Flooding rates for operation of the 24 ft column with no scrubbing or mass transfer (recycle feed) ranged from 665 to > 1770 gal ft^{-2}hr^{-1}, as the pulse frequency decreased from 90 to 50 cpm and are in good agreement with values obtained with mass transfer (Figure 4.1). Increasing the ratio of the dispersed phase to the continuous phase from 3/10 to 3/1, while holding the pulse frequency constant at 70 cpm, lowered the flooding rate from 933 to 287 gal ft^{-2}hr^{-1}.

The flooding rate determined for the 24 ft column of 933 gal ft^{-2}hr^{-1} at 70 cpm checked the 950 gal ft^{-2}hr^{-1} at 70 cpm value obtained in a 12 ft column.

4.2 Correlation of Data

Flooding data was correlated using the method of Logsdail and Thornton[1] whereby phase flow rates were related to the dispersed phase holdup, x, and the characteristic droplet velocity, $\bar{V}_o$, by means of Eq. 1

$$\frac{V_d}{x} + \frac{V_c}{(1 - x)} = \bar{V}_o (1 - x) \qquad (1)$$

V_d = velocity of dispersed phase, ft/hr

V_c = velocity of continuous phase, ft/hr

x = fraction dispersed phase holdup

$\bar{V}_o$ = characteristic droplet velocity, ft/hr

[1] "Liquid-Liquid Extraction, Part XIV, The Effect of Column Diameter Upon the Performance and Throughput of Pulse Plate Columns," Logsdail, D. H. and Thornton, J. D., Trans., Inst. Chem. Engrs. Vol 35: 331-342 (1957).

Table 4.1. Physical Properties of Test Solutions

Solution	Density g/ℓ	Viscosity centipoise	Composition
U-Feed	1.275	4.442	U, 2.1 g/ℓ, H^+, 0.17 M $Al(NO_3)_3$, 1.75 M
Scrub	1.155	2.177	1.0 M $Al(NO_3)_3$, H^+, 0.03 AD
Solvent	0.765	1.42	5% TBP in Amsco 125-82
Recycle Feed	1.275	3.425	1.75 M $Al(NO_3)_3$, 0.16 M H^+

Solution Pairs	Interfacial Tension dynes/cm
Solvent) Raffinate)	17.1
Solvent) Recycle Feed)	16.5
Loaded Solvent) Scrub)	17.1

All measurements at 25°C.

Table 4.2. Flooding Point Data

Run No.	Pulse Frequency cpm	Phase Ratio Solvent	Phase Ratio Scrub	Phase Ratio Feed	Flooding Rate gal $ft^{-2}hr^{-1}$
	24 ft Compound Extraction Scrub Column-U Feed				
1	50	3	0.1	10	2010
2	70	3	0.1	10	1020
3	90	3	0.1	10	580
	24 ft Column - Recycle Feed				
7	50	3		10	> 1770
8	70	3		10	933
6	90	3		10	665
9	70	1		1	615
12	70	2		1	400
10	70	3		1	287
11	50	3		1	450
	12 ft Column - Recycle Feed				
13	170	3		10	950

Pulse amplitude = 1 inch

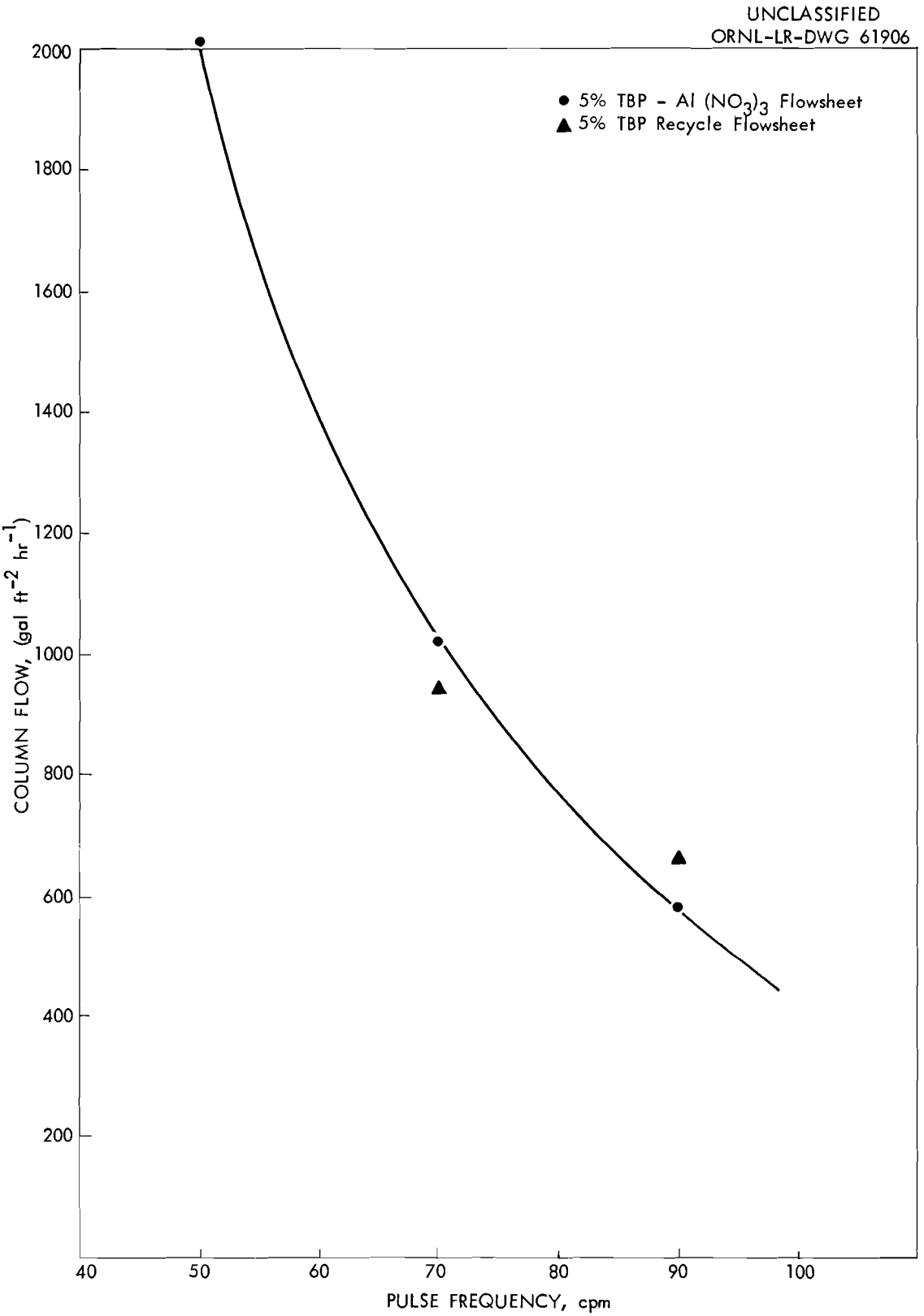

Fig. 4.1. Flooding curve - sieve plate extraction column.

Plotting the values of $V_d + V_c x/(1 - x)$ vs $x(1 - x)$ calculated from the flooding test data resulted in a series of straight lines passing through the origin whose slope = $\overline{V}_o$, (Figures 4.2 and 4.3, Table 4.3). The limiting fractional holdup at flooding can be calculated by Eq. 2.

$$x_f = \frac{\left[\left(\frac{V_d}{V_c}\right)^2 + 8\left(\frac{V_d}{V_c}\right)\right]^{1/2} - 3\,\frac{V_d}{V_c}}{4\left(1 - \frac{V_d}{V_c}\right)} \qquad (2)$$

where V_d/V_c is the ratio of the dispersed phase flow to the continuous phase flow. Using the limiting x_f values and $\overline{V}_o$ values, the theoretical flooding velocities can be calculated using Eqs. 3 and 4.

$$V_d = 2\overline{V}_o\, x_f^{\,2}\left(1 - x_f\right) \qquad (3)$$

$$V_c = \overline{V}_o\left(1 - x_f\right)^2\left(1 - 2x_f\right) \qquad (4)$$

The actual and theoretical phase velocities at flooding agreed quite well for the 3/10 phase ratio tests (Table 4.4). However, as the ratio of the dispersed phase to the continuous phase increased, the theoretical flooding velocities became progressively greater than those actually measured. For simplicity, the above correlation assumed that the holdup of the dispersed phase was constant throughout the column. Actually, holdup of the dispersed phase varied markedly (Figure 4.4), consequently flooding occurred at some point in the column at a lower dispersed phase velocity than predicted. Probably the surface effects of the plates where local flooding occurred were different from those of the majority of plates in that they tended to form smaller dispersed phase droplets, resulting in increased holdup. Further, as the ratio of dispersed phase to continuous phase increases, these surface effects would become increasingly important and actual flooding values should be progressively lower than the predicted values, similarly to the results shown in Table 4.4.

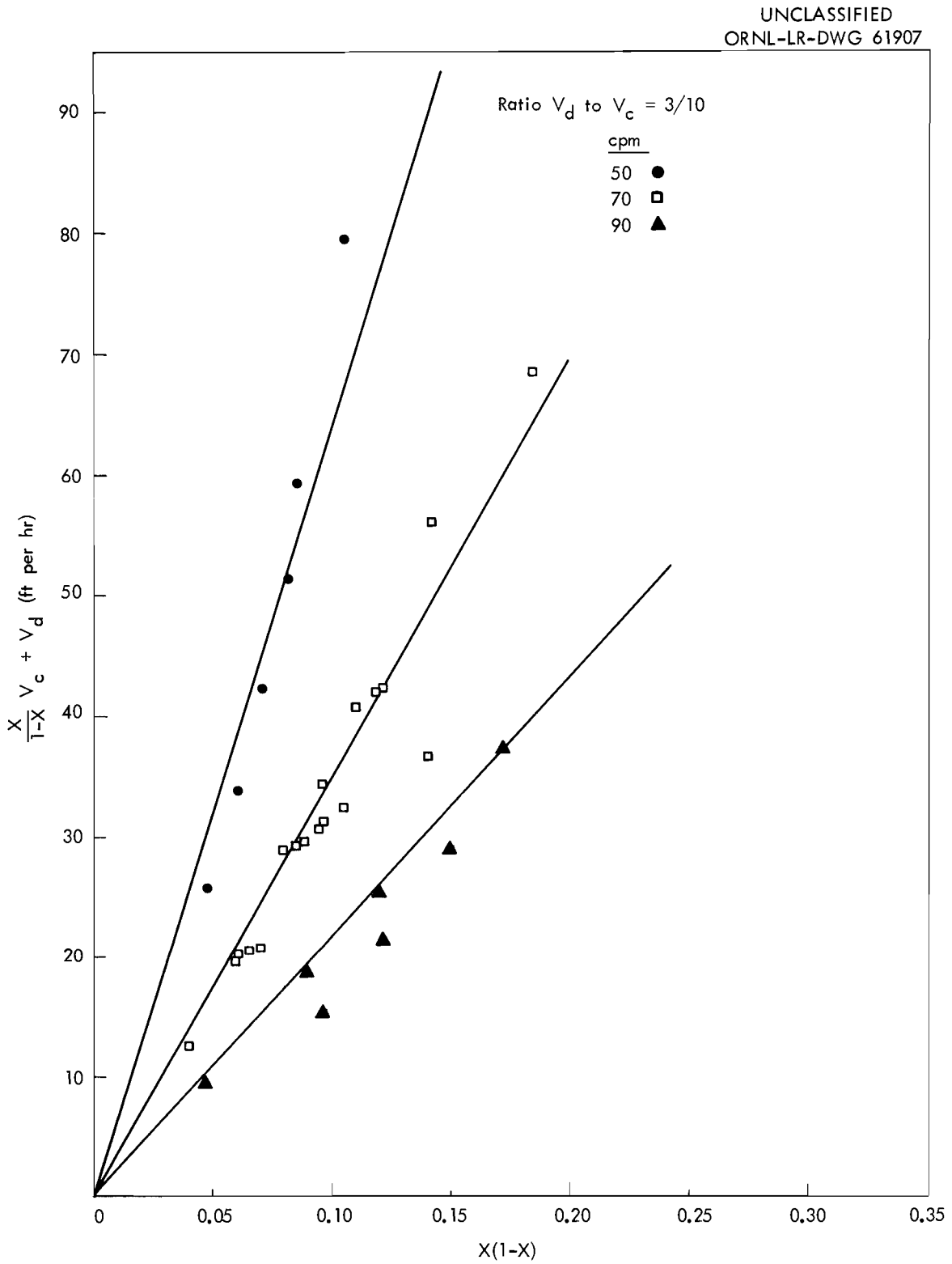

Fig. 4.2. Characteristic droplet velocity curves.

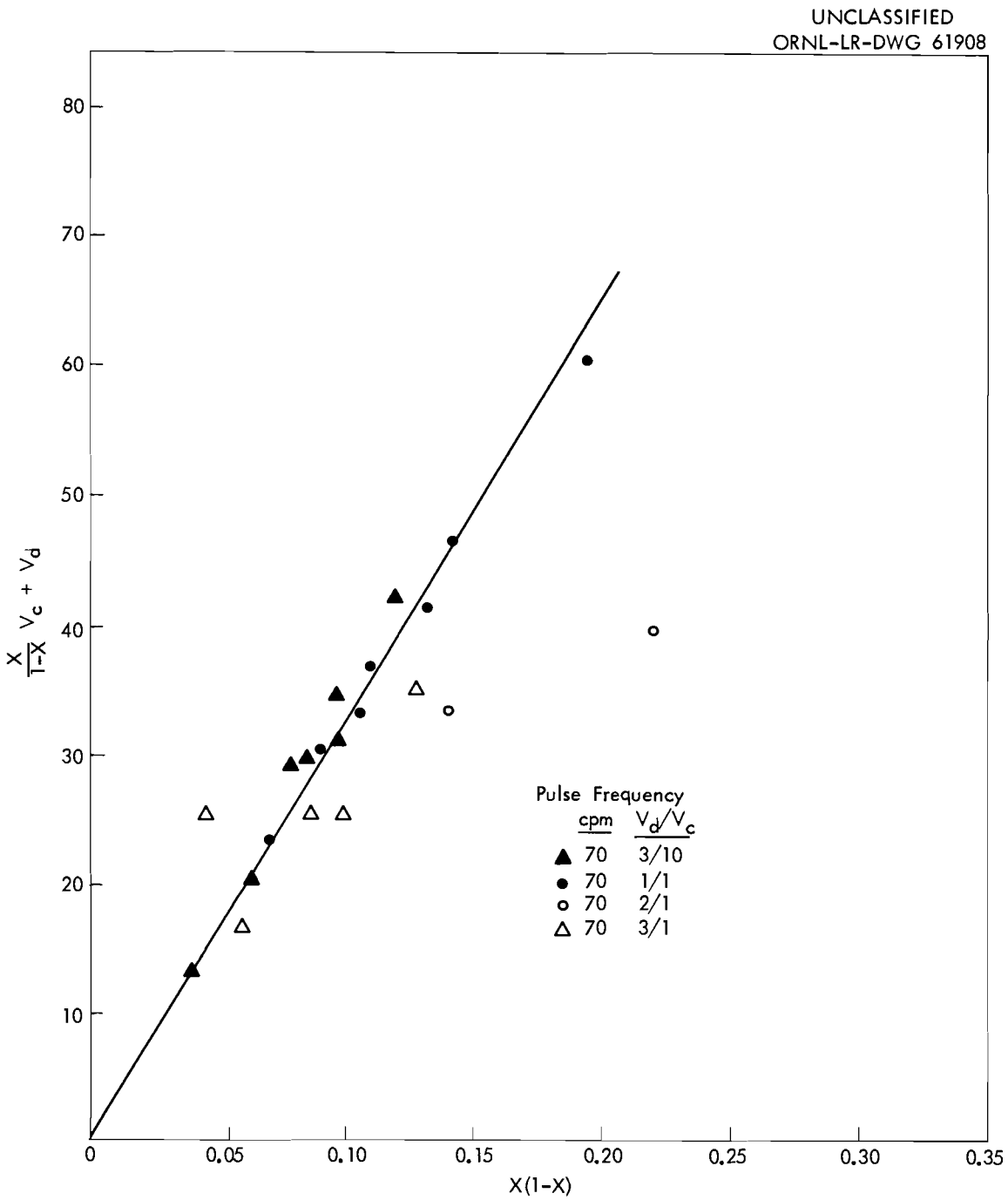

Fig. 4.3. Characteristic droplet velocity curves.

Table 4.3. Recycle Flooding Test

Run No.	Pulse Frequency cpm	Phase Ratio V_d/V_c	Run Time hr	Dispersed Phase Flow Rate V_d, ft/hr	Fraction Holdup x	x(1 - x)	$\frac{x}{(1 - x)} V_c + V_d$
7	50	3/10	0.5	22.0	0.050	0.047	25.8
			0.5	27.5	0.065	0.061	33.9
			0.5	33.0	0.078	0.072	42.4
			0.5	38.5	0.090	0.082	51.2
			0.5	44.0	0.094	0.085	59.2
			0.5	55.0	0.119	0.105	79.6
8	70	3/10	0.5	11.0	0.042	0.040	12.6
			0.5	16.5	0.069	0.064	20.6
			0.5	22.0	0.087	0.080	29.1
			1.0	22.0	0.094	0.085	29.6
			1.0	22.0	0.107	0.096	30.8
			1.0	24.8	0.107	0.096	34.6
			0.5	27.5	0.138	0.119	42.1
6	90	3/10	0.5	8.3	0.050	0.048	9.7
			0.5	11.0	0.107	0.096	15.4
			0.75	13.8	0.099	0.089	18.9
			1.0	13.8	0.142	0.121	21.3
			0.5	16.5	0.142	0.121	25.6
			1.0	16.5	0.184	0.150	28.9
			0.5	19.3	0.222	0.173	37.5
9	70	1/1	0.5	22.0	0.077	0.071	23.8
			0.5	27.5	0.099	0.090	30.5
			0.5	33.0	0.127	0.110	37.8
			0.5	35.8	0.160	0.134	41.4
			0.5	38.5	0.172	0.142	46.5
			0.5	44.0	0.268	0.196	60.1
10	70	3/1	1.0	16.5	0.065	0.061	16.9
			0.5	24.8	0.048	0.046	25.2
			0.5	24.8	0.096	0.086	25.6
			1.0	24.8	0.111	0.099	25.8
			0.5	33.0	0.149	0.127	34.9
11	50	3/1	1.0	33.0	0.107	0.096	34.3
			0.5	49.5	0.168	0.140	52.8
			1.0	49.5	0.230	0.177	54.4

Table 4.3. (Cont'd)

Run No.	Pulse Frequency cpm	Phase Ratio V_d/V_c	Run Time hr	Dispersed Phase Flow Rate V_d, ft/hr	Fraction Holdup x	x(1 - x)	$\frac{x}{(1 - x)} V_c + V_d$
12-A	70	2/1	0.5	33.0	0.170	0.140	33.3
			1.0	33.0	0.170	0.140	33.3
			1.0	38.5	0.320	0.221	39.1
12-B	70	1/1	0.5	27.5	0.122	0.107	31.3
12-C	70	3/10	1.0	27.5	0.229	0.176	54.8
			1.0	33.0	0.153	0.130	52.9
			0.5	16.5	0.073	0.067	20.8
			0.5	22.0	0.107	0.096	30.8
			1.0	22.0	0.122	0.107	32.2
			4.0	22.0	0.168	0.140	36.8
13*	70	3/10	0.5	16.5	0.063	0.059	20.2
			1.0	16.5	0.063	0.059	20.2
			0.5	22.0	0.094	0.085	29.6
			1.0	22.0	0.094	0.085	29.6
			0.5	27.5	0.126	0.110	40.7
			1.0	27.5	0.141	0.121	42.6
			0.5	33.0	0.243	0.184	68.4
			1.0	33.0	0.173	0.143	56.0

*Run No. 13 in 12 ft column.

Pulse amplitude 1 inch - Aqueous continuous operation

Table 4.4. Calculated and Actual Flow Rates at Flooding

Phase Ratio V_d/V_c	Fractional Holdup x_f	Pulse Frequency cpm	$\bar{V}_o$ ft/hr	Calculated V_d ft/hr	Actual V_d ft/hr
3/10	0.242	50	640	56.9	>55.5
		70	350	31.1	28.8
		90	220	19.5	20.6
1/1	0.333	70	330	48.9	41.3
2/1	0.382	70	240	43.3	35.8
3/1	0.407	50	350	68.7	45.3
		70	280	55.0	28.9

Pulse amplitude = 1 inch

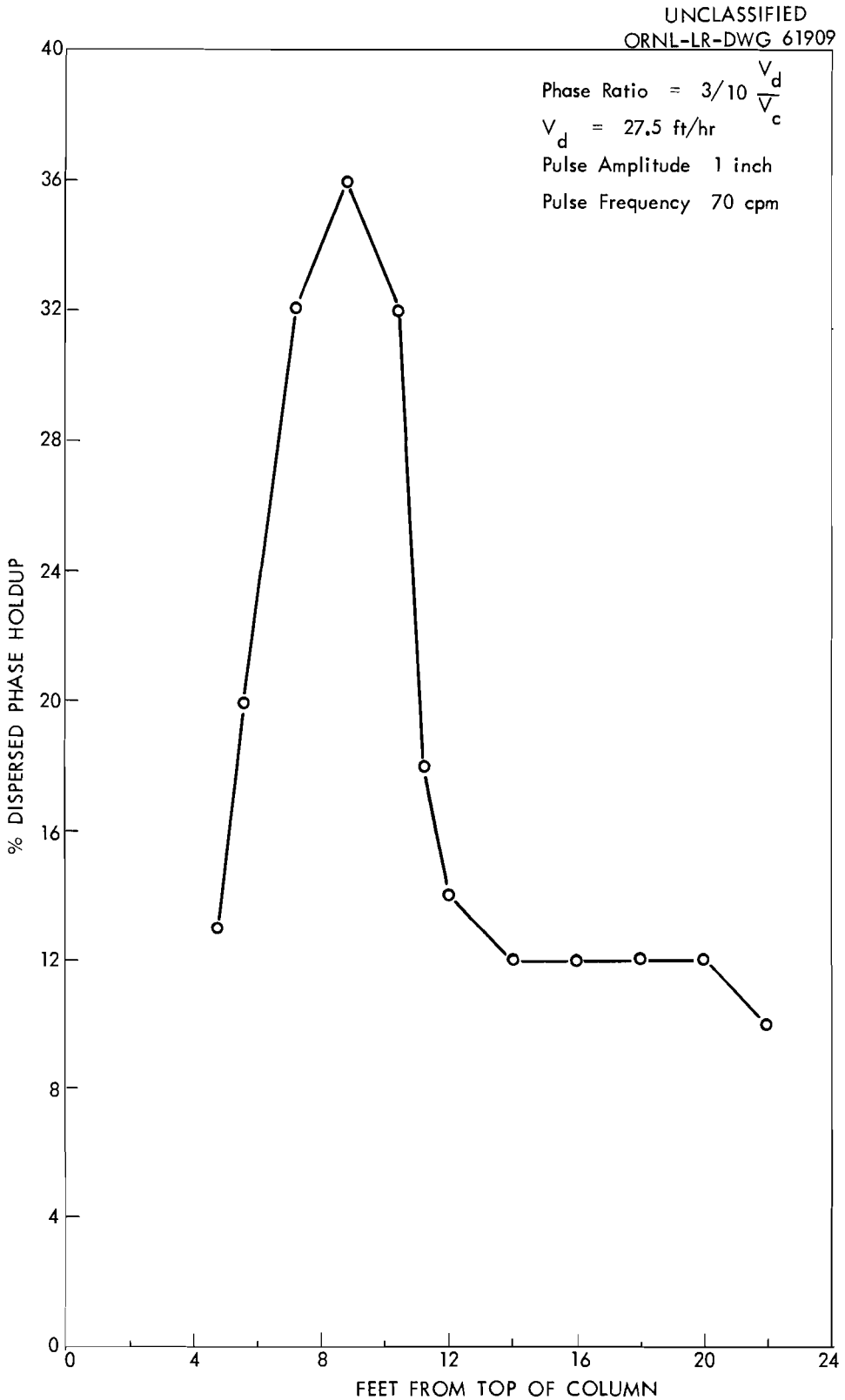

Fig. 4.4. Holdup profile in sieve plate column.

5.0 WASTE PROCESSING

J. C. Suddath

The purpose of this program is to obtain engineering information for design of a hot pilot plant, which will demonstrate the disposal of high level waste solutions. During this period the main emphasis was on the close coupled evaporator-calciner with Purex type feed.

5.1 Evaporator-Calciner Test R-37 - C. W. Hancher

The purpose of this test (R-37) was to demonstrate the operability and control of a close coupled waste evaporator and calciner, previously described, March and April 1961 Unit Operations monthly reports. The evaporator had an operating capacity of 22 liters. The calciner pot was 8-in.-dia by 94-in. long, operating capacity of about 60 liters.

The feed used was simulated Purex 1WW (40/ton of U) plus 1.2 M of Na and 0.2 M Mg added to reduce sulfate volatility, Table 5.1. Sodium was added as Na_2SO_4 and the Mg as 0.1 M $MgSO_4$ and 0.1 M as MgO in the simulated feed with this being the only sulfate in feed. The analytical laboratory had difficulty in determining Mg in the feed samples, but the correct amount was added during feed make-up for the amount of sulfate, since the only sulfate in the feed was added either as Na_2SO_4 or $MgSO_4$.

5.2 Evaporator-Calciner Control and Operation

Test R-37 started with the evaporator filled with cold feed and the calciner empty and cold (Table 5.2). The evaporator contents are heated to boiling and then the calciner is heated and filled simultaneously, requiring about 30 min to fill the calciner. As the control variables reach their set point conditions they were switched from manual to automatic control. The control settings for five controlled streams are shown in Table 5.3. The system controlled satisfactory for over 90% of the test (Table 5.4), during one period (test time 6.0) calciner liquid level probe plugged for a short period of time, about 5 min. The control was shifted to the higher elevation liquid level probe, Figure 5.1. By the time the probes were switched the calciner level was low and the evaporator level had drifted high and was boiling at a high rate (4 - 6 liters/min) to reduce the level. The calciner removed a significant volume from the evaporator at a high rate and overshot slightly. The calciner and evaporator liquid levels oscillated for about 3 hrs, before it was manually brought back into control in a few minutes. Major upsets had to be controlled manually.

The feed rates varied from 4 to 70 liters/hr, the average rate was 21.0 liters/hr. The water addition rate was 3 to 172 liters/hr. The water is added to remove the nitric acid from the evaporator by steam stripping. Evaporator acid is held at 6 M or below to reduce Ru volatility, no cold or radioactive Ru was used in this test. The water to feed ratio was 0.05 to 5.80, the average ratio was 2.4, Figure 5.2. The concentration of evaporator acid was controlled by evaporator temperature and water addition. The evaporator temperature set point was 113°C, which was predetermined to be approximately 6 M HNO_3 at -0.5 psig and a Fe concentration 25 to 30 g/liter.

Table 5.1. Test R-37 Feed-Purex (40 gal/ton U)

	H	NO_3	Fe	Al	SO_4	Na	Mg
As made up	4.1	6.1	0.5	0.1	1.0	1.8	0.2
As analyzed							
Tank 1	3.6-4.3	6.0-6.1	0.49-0.51	0.11	1.0-1.1	1.6-1.8	0.09-0.11
Tank 2	3.6-4.3	6.1	0.49	0.11	0.98-1.1	1.6-1.8	0.08-0.11
Tank 3	3.4-4.2	6.1	0.48-0.49	0.11	1.0	1.2-1.8	0.11-0.18

Table 5.2. Test R-37 Operation Log

Time Hour	Test Time Hour		
9:00 A	0	Start:	Empty-cold calciner Full-cold evaporator
9:30 A	0.5		Calciner full
11:30 A	2.5		Calciner liquid level probe plugged
12:00 A	3.0		Calciner liquid level probe plugged Added 50 cc/min water
3:00 P	6.0		Calciner liquid level went high, plugged probe, when unplugged then low. Meanwhile evaporator went high, started to boil fast, then filled the calciner and went low. Cycle repeated. Took 3 hrs to return to good control.
7:00 P	10.0		Water to evaporator manual (20 liter/hr)
12:00 A	15.0		Everything normal, calciner feed rate low
4:00 A	19.0	Stop:	Stopped feeding calciner
6:00 A	20.0	Stop:	Stopped evaporator operation
6:00 A	20.0	Stop:	Stopped calcination

Table 5.3. Control Setting for Test R-37

	Control Variable	Control Range 0-100%	Prop. Band %	Reset min	Set Point %	Dev* from Set Point %
Evaporator	Liq Level	7.4-35.0 liter	100	10	50	40-85
Evaporator	Density	1.0-1.5 g/cc	200	10	65***	57-71
Evaporator	Temperature	101-128°C	100	10	50	30-90
Evaporator	Pressure	-5 to +5 psig	50	0.3	40	40-60
Calciner	Liq Level	44-52 liter	25	3	50	48-62**

* Deviations of hourly reading
** At end of test went to 100% full
*** Approximately 30 g/liter Fe

Table 5.4. Operational Limits for Test R-37

		Limit "A" Upper Operational Limit	Limit "B" Upper Desired Limit	Set Point	Limit "C" Lower Desired Limit	Limit "D" Lower Operational Limit	Operational* Reading min	Operational* Reading max
Evap.	(scale %	90	65	50	35	25	40	85
Liq Level	(liters	33	26	22	18	15	19	31
Evap.	(scale %	80	70	65	50	40	57	71
Density	(g/cc	1.40	1.35	1.32	1.25	1.20	1.27	1.36
Evap.	(scale %	90	60	50	20	0	30	90
Temp.	(°C	122	115	113	107	103	109	122
Evap.	(scale %	45	42	40	38	35	40	60
Pressure	(psig	-0.5	-0.75	-1.0	-1.25	-1.5	-1.0	+1.0
Calciner	(scale %	30	40	50	60	70	48	62
Liq Level	(liters	58	59	60	61	62	59	61

* Recorded hourly reading

UNCLASSIFIED
ORNL-LR-DWG 61910

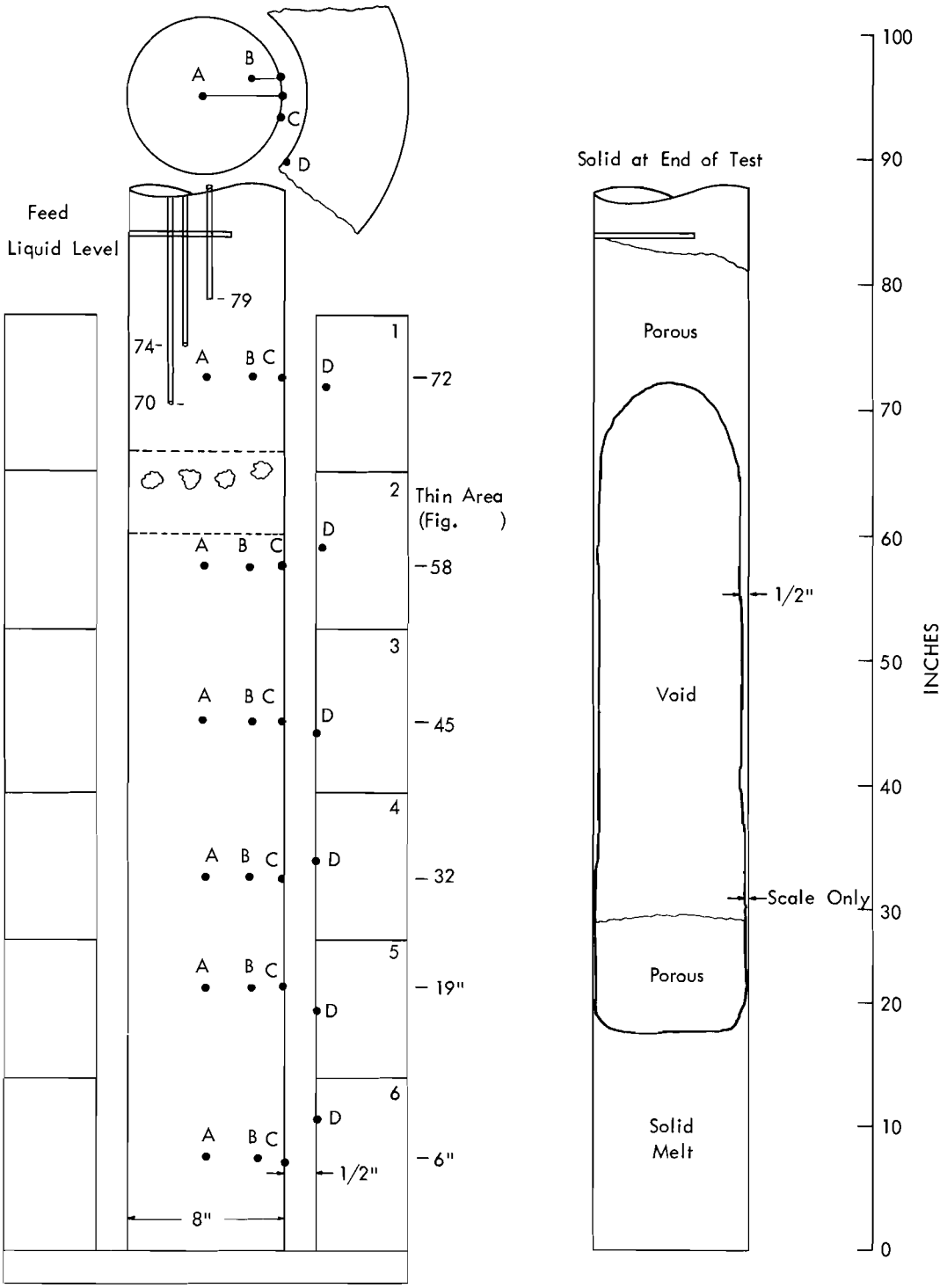

Fig. 5.1. Calciner pot R-37.

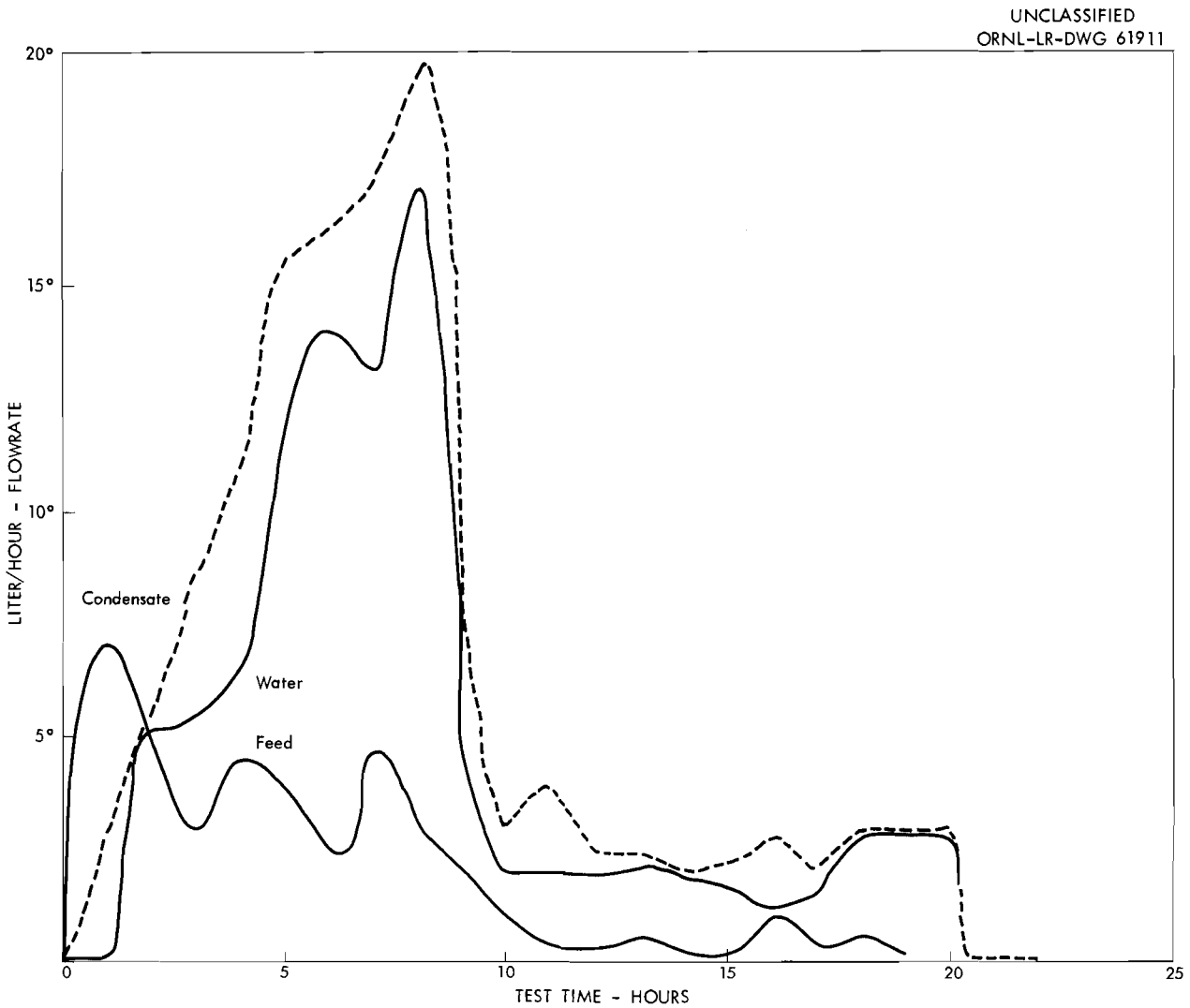

Fig. 5.2. Test - R-37. Feed, water, and condensate flowrates as a function of time.

The control of variables has been evaluated by the setting of limits:

Limit "A" Too high, out of control, dangerous
Limit "B" Upper limit of good control
Limit "C" Lower limit of good control
Limit "D" Too low, out of control, uneconomical

The evaporator temperature control was very good. Only two high readings, once above "A" limit and once above "B" limit, and no low readings, Figure 5.3. However the actual acid concentration deviated more than the temperature indicated deviation, Figure 5.3. The one high acid concentration was probably due to a low Fe concentration below limit "C" at that time.

The density of evaporator content was used to determine the dissolved solids as nitrate salts which in turn were expressed as Fe concentration since Fe is the major consistent. When the density was low, feed was added to the evaporator. The density was twice above limit "B", this was the only control difficulty (Figure 5.4). However, the Fe concentration was below limit "C" twice and above limit "B" once. The density and Fe concentration followed each other very well.

The evaporator pressure controlled very well (Table 5.3): 90% of the time the process controlled -1.0 $\pm$ 0.25 psig.

The nitrate in the condensate was 72% of the nitrate in the feed. The remaining NO_3 is assumed to be in the solid, since it is not completely calcined. The sulfate in the condensate was 0.75% of the feed, and the sulfate in the solid was 92% of the feed.

The non-condensable off-gas was 391 cu ft or 0.97 cu ft/liter of feed. This is about 4 to 5 times the volume of non-condensable off-gas from test R-36 (Table 5.5).

5.3 Calciner Pot Corrosion

In all of the other pot calcination test made to date, corrosion has not been serious. In test R-37 a number of holes (5 to 8) about 2-in. dia corroded through the calciner pot at 60 to 65 in. from the bottom of the pot. There also was local overheating in this area of the calciner pot from furnace section No. 2, Figure 5.1.

There are 5 thermocouples per furnace section:

A = center of pot - record
B = inside 1 in. from wall of pot - record
C = outside of pot - record
C = outside of pot - control
C = in furnace section - control

The power to the furnaces was controlled by a thermocouple attached to the outside of the calciner pot at a set point of 900°C. The furnace thermocouple in the furnace was to limit its temperature to about 1150 to 1200°C.

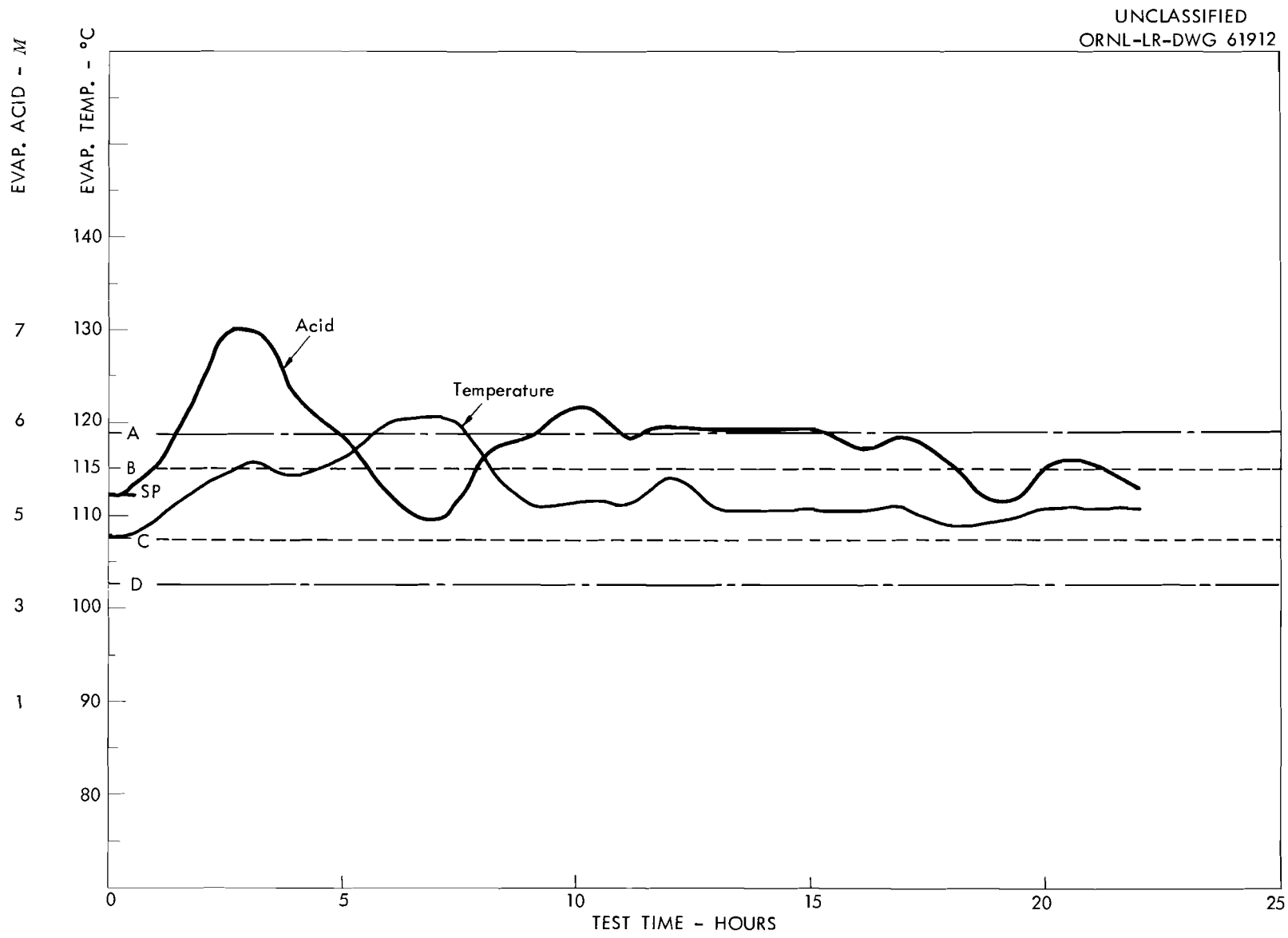

Fig. 5.3. Evaporator-calciner test - R-37. Evaporator acid and evaporator temperature as a function of test time.

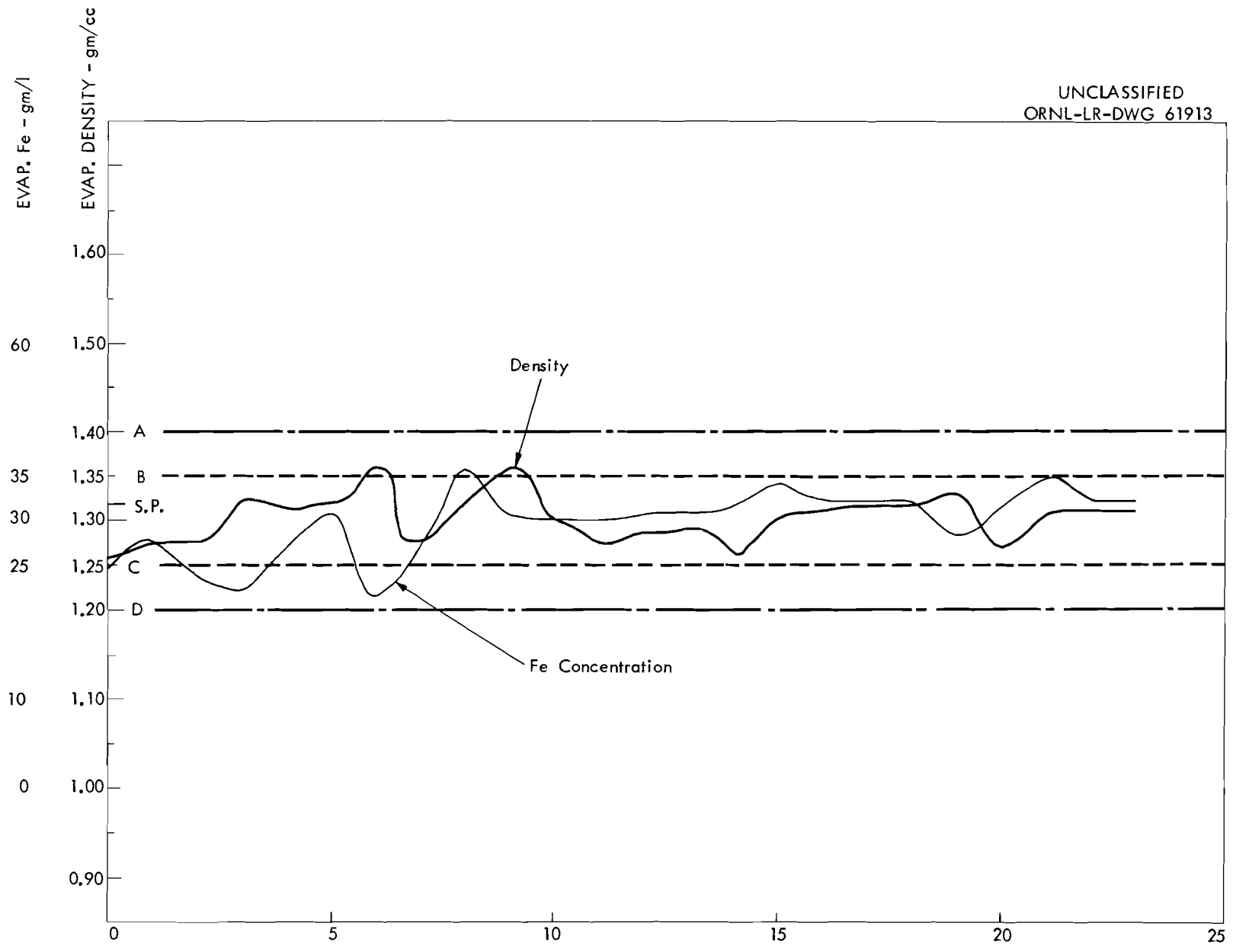

Fig. 5.4. Test R-37. Evaporator density and iron can as a function of test time.

Table 5.5. Test R-37 - System Results

Nitrate Balance

System input 2469 g moles
System recovery
(condensate - 1776 g mol = 72%
(off-gas - unknown
(solid - 86 g mol = 3.5%

Sulfate Balance

System input 390 g mole
System recovery
(condensate - 5.0 g mol = 0.75%
(off-gas - unknown
(solid - 360 g mol = 92.0%

Off-Gas

831 cu ft total
440 cu ft leakage and gas purge (20 cu ft/hr, 25% and 75%)

391 cu ft of generated non-condensables

391/404 = 0.97 cu ft/liter of system feed

Feed Rate

404 liter/19 hr = 21.0 liters/hr

Water Rate

983 liter of water; water to feed ratio = 983/404 = 2.4

Calcined Solids

78 kg solids/68 liter = 1.15 g/cc bulk density

At test time 17.0 all of thermocouples appeared to be operating satisfactorily. Apparently thermocouple (58-in. - C) to the Wheelco control for the furnace section No. 2 was then destroyed by corrosion and reported a low temperature which caused furnace section No. 2 to overheat, (Table 5.6). The overheating occurred after the pot had corroded through. The pot was 100 mil 304L stainless steel. The area at the elevation around the holes was reduced to about 25 mil thickness (Figure 5.5).

One possible explanation of the corrosion is that $MgSO_4$ decomposed at 900°C, freeing SO_3, which mixed with HNO_3 available at the corroded zone. The corroded zone was approximately the operating liquid level. In R-36 with no Mg or Na there was plenty of SO_4 to corrode completely the ends of the liquid level probes and feed lines, but the wall was not attacked (Table 5.6). In R-37 the feed and level lines were not corroded. Complete data over the feeding cycle are presented in Table 5.7.

Calcined Solid. The calcined solids had a bulk density of 1.15 g/cc (Table 5.5). When the calciner pot was slit from end to end and half of the metal shell removed (Figure 5.6), it was noted that the midsection of the calciner was empty except for a thin outer film from 1/4 to 1/2 in. thick. The bottom appears to have melted (Figure 5.7). The top (Figure 5.8) had not been calcined. The solid was red-yellow and smelled of sulfur.

Table 5.6. Temperature Test Time 17.0 to 20.0 at the Top of Calciner

Inches from Bottom	Thermocouples - (Figure 5.1) A °C	B °C	C °C	D °C
72	120 → 120	500 → 550	920 → 925	1125 → 1150
58	200 → 960	840 → 1050	980* → 1060	1000 → 1040
45	915 → 1000	830 → 1000	1000 → 950	900 → 850

← Calciner Wall

* Thermocouple (58 in. - C) to Wheelco control was corroded into when calciner pot was removed from the furnace after the test.

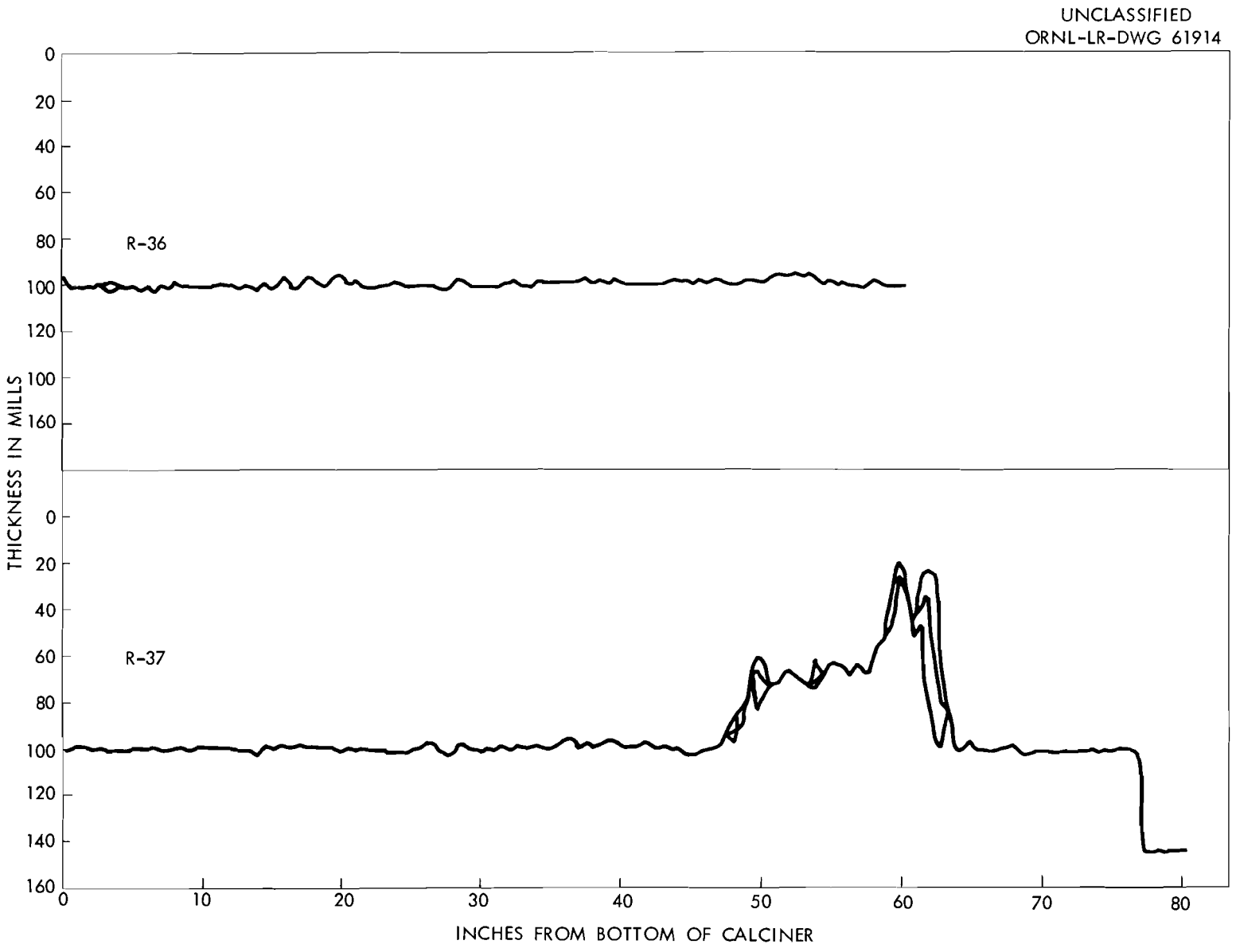

Fig. 5.5. Thickness of calciner pots after testing.

Table 5.7. Waste Evaporator-Calciner Test R-37 (Purex Waste)

						Purex Waste (40 gal/ton) + 1.2 M Na and 0.2 M Mg									
Test Time	System Feed Purex	System Water Feed	Water To Feed Ratio	System Condensate	System Off-gas	Mol NO_3 Input	Mol NO_3 Condensate	Evap. Density	Evap. Temp.	Evap. Fe Conc.	Evap. Acid	Evap. Steam Temp.	Calciner Heat Input	Calciner Temp. at Feed Point	Calciner Temp. Midsection Center
hrs	liters	liters	Ratio	liter	cu ft*	g mol	g mol	g/cc	°C	g/ℓ	mol	°C	KWH	°C	°C
1	70	0	0	29	35	430	24	1.27	109	26	5.4	117	51	115	115
2	121	3	0.06	83	64	743	165	1.27	113	23	6.1	134	97	125	125
3	150	57	1.9	166	91	921	530	1.32	116	22	7.9	112	141	120	125
4	196	123	1.5	277	128	1197	770	1.31	114	27	9.0	134	185	120	430
5	235	241	3.0	434	170	1436	878	1.32	116	31	7.5	136	218	120	370
6	259	381	5.8	598	217	1577	1026	1.36	120	22	6.7	154	251	125	250
7	305	512	2.8	775	268	1859	1141	1.27	122	27	5.4	158	279	130	300
8	335	684	5.7	977	313	2043	1369	1.32	116	36	4.9	136	308	120	415
9	356	736	2.5	1050	362	2173	1445	1.36	111	32	6.2	112	329	120	765
10	366	756	2.0	1080	408	2234	1486	1.30	112	30	6.6	116	348	115	910
11	370	791	8.7	1119	450	2258	1544	1.27	112	30	7.2	117	362	115	920
12	374	811	5.0	1143	492	2283	1575	1.28	114	31	6.6	117	368	115	920
13	379	830	4.7	1167	537	2314	1604	1.28	111	31	6.9	113	379	115	920
14	381	848	9.0	1187	581	2326	1627	1.26	111	32	6.8	113	388	115	925
15	383	867	9.0	1208	625	2339	1651	1.30	111	34	6.8	116	399	120	925
16	393	884	1.7	1235	668	2400	1675	1.32	111	32	6.9	115	415	120	930
17	397	900	4.0	1250	705	2425	1691	1.32	111	32	6.4	113	426	120	925
18	402	912	2.4	1267	733	2455	1707	1.33	108	32	6.6	111	434	120	920
19	404	927	7.5	1284	764	2468	1719	1.27	109	28	6.1	111	444	120	930
20	-	955	-	1312	792	-	1752	1.31	112	32	5.2	120	453	120	930
21	-	983	-	1345	819	-	1776	1.31	112	35	6.1	123	461	120	935
22	-	983	-	1345	831	-	1776	1.31	112	31	6.1	123	466	120	935

* System leakage and purging = 20 cu ft/hr

UNCLASSIFIED
PHOTO 53762

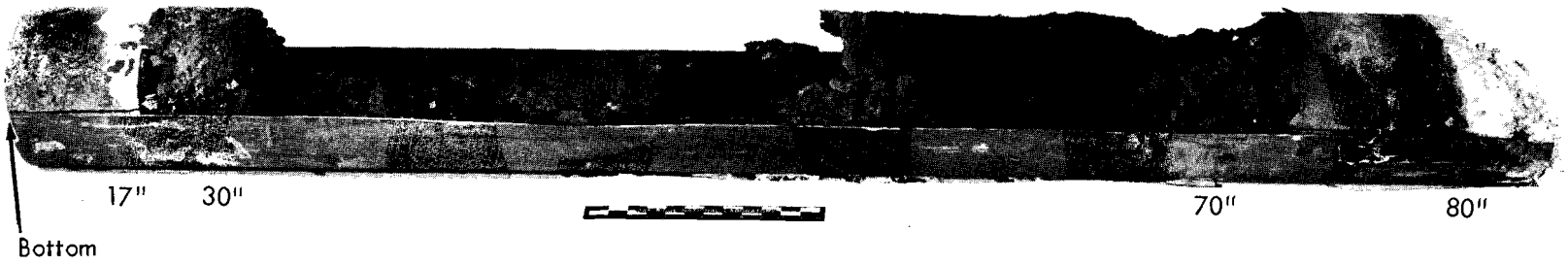

Fig. 5.6. Calcined solids R-37.

UNCLASSIFIED
PHOTO 53768

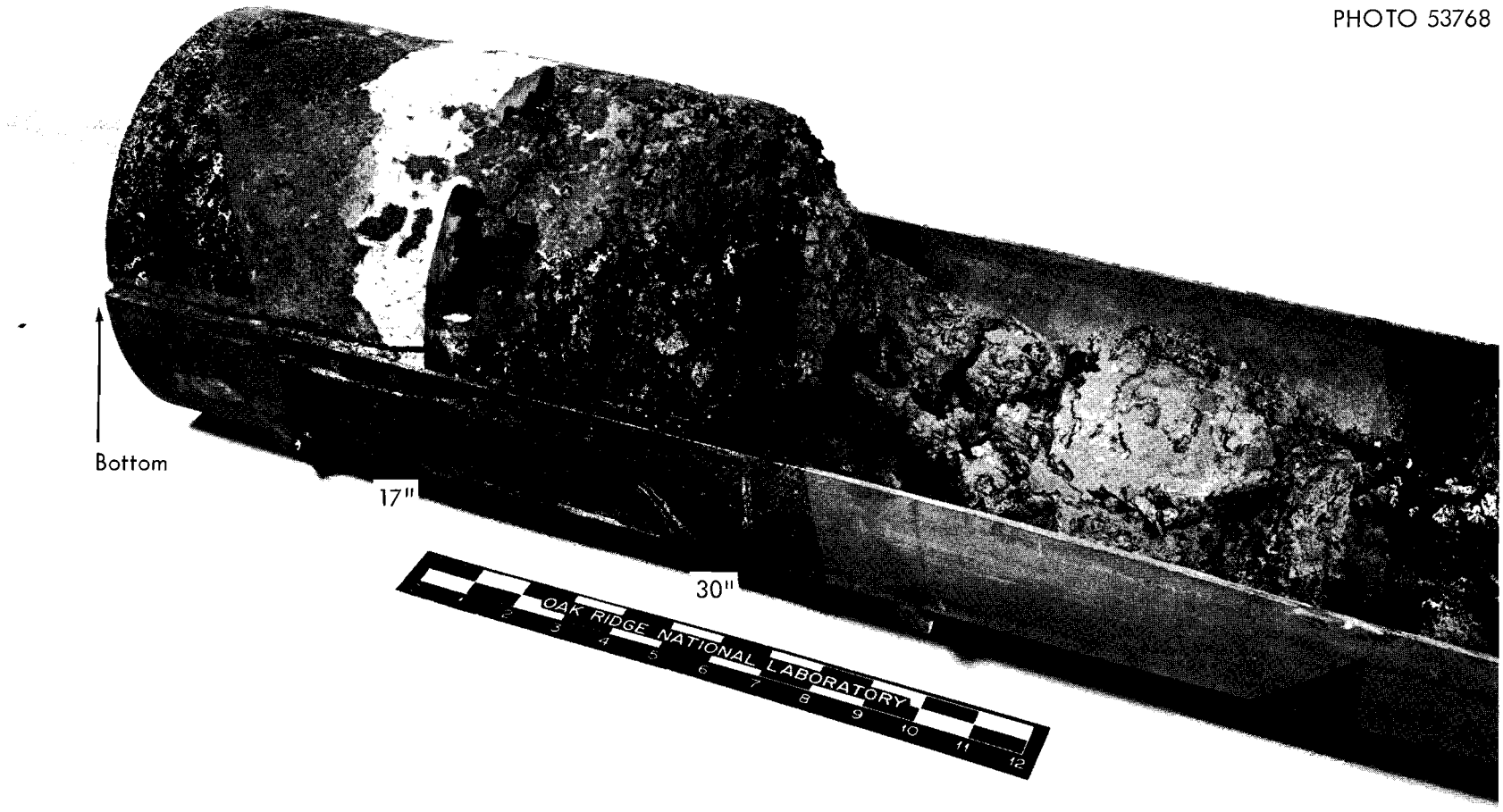

Fig. 5.7. Calcined solids R-37.

UNCLASSIFIED
PHOTO 53765

Fig. 5.8. Calcined solids R-37.

DISTRIBUTION

1. E. L. Anderson (AEC Washington)
2. F. P. Baranowski (AEC Washington)
3. W. G. Belter (AEC Washington)
4. S. Bernstein (Paducah)
5. R. E. Blanco
6. J. O. Blomeke
7-10. J. C. Bresee
11. R. E. Brooksbank
12. K. B. Brown
13. F. R. Bruce
14. J. A. Buckham (ICPP)
15. L. P. Bupp (HAPO)
16. W. D. Burch
17. W. H. Carr
18. G. I. Cathers
19. J. T. Christy (HOO)
20. W. E. Clark
21. V. R. Cooper (HAPO)
22. K. E. Cowser
23. F. E. Croxton (Goodyear Atomic)
24. F. L. Culler, Jr.
25. W. Davis, Jr.
26. O. C. Dean
27. D. E. Ferguson
28. L. M. Ferris
29. R. J. Flanary
30. E. R. Gilliland (Consultant MIT)
31. H. E. Goeller
32. M. J. Googin (Y-12)
33. H. B. Graham
34. A. T. Gresky
35. P. A. Haas
36. M. J. Harmon (HAPO)
37. F. E. Harrington
38. L. P. Hatch (BNL)
39. O. F. Hill (HAPO)
40. J. M. Holmes
41. R. W. Horton
42. A. R. Irvine
43. G. Jasny (Y-12)
44. H. F. Johnson
45. W. H. Jordan
46. S. H. Jury
47. K. K. Kennedy (IDO)
48. B. B. Klima
49. E. Lamb
50. D. M. Lang
51. S. Lawroski (ANL)
52. R. E. Leuze
53. W. H. Lewis
54. J. A. Lieberman (AEC Washington)
55. R. B. Lindauer
56. A. P. Litman
57. J. T. Long
58. B. Manowitz (BNL)
59. J. L. Matherne
60. J. A. McBride (ICPP)
61. J. P. McBride
62. W. T. McDuffee
63. R. A. McGuire (ICPP)
64. R. A. McNees
65. R. P. Milford
66. J. W. Morris (SRP)
67. E. L. Nicholson
68. J. R. Parrott
69. F. S. Patton, Jr. (Y-12)
70. H. Pearlman (AI)
71. R. H. Rainey
72. J. T. Roberts
73. K. L. Rohde (ICPP)
74. C. A. Rohrmann (HAPO)
75. A. D. Ryon
76. W. F. Schaffer, Jr.
77-79. E. M. Shank
80. M. J. Skinner
81. C. M. Slanksy (ICPP)
82. S. H. Smiley (ORGDP)
83. J. I. Stevens (ICPP)
84. C. E. Stevenson (ANL, Idaho)
85. K. G. Steyer (General Atomics)
86. E. G. Struxness
87. J. C. Suddath
88. J. A. Swartout
89. F. M. Tench (Y-12)
90. V. R. Thayer (duPont, Wilmington, Del
91. W. E. Unger
92. J. Vanderryn (AEC ORO)
93. F. M. Warzel (ICPP)
94. C. D. Watson
95-124. M. E. Whatley
125. G. C. Williams
126. R. H. Winget
127. C. E. Winters
128. R. G. Wymer
129-130. Central Research Library
131-134. Laboratory Records
135. Laboratory Records (RC)
136. Document Reference Section
137. Research and Development Division
138-152. DTIE